
# Implementation and testing of photovoltaic Power Plant Control in a scaled platform

Robin Bourgeon

Master's thesis – Master in Energy Engineering
Spring semester, 2017 – UPC-ETSEIB

Thesis work carried out in the laboratory CITCEA-UPC under the supervision and guidance of Eduard Bullich-Massagué and Josep Andreu Vidal

# Abstract

Grid code requirements have become more demanding with the increasing penetration of renewable power plants, as they are starting to be used for ensuring grid support. As a result, the power plant control (PPC) of photovoltaic (PV) plants is a critical issue for ensuring the stability of these plants and their appropriate grid integration. This Master's thesis focuses on the implementation of a PPC algorithm for an hybrid battery-PV power plant, including active power ramp rate limitation and battery state of charge control. This algorithm is first tested in a simulation software using a dynamic plant model, and then on a scaled microgrid emulation platform that emulates the behaviour of a PV plant.

# Contents

# List of Figures

# Nomenclature

| | | | |
|---|---|---|---|
| PV | photovoltaic | PCC | Point of Common Coupling |
| | | $T_w$ | Time window |
| $T_s$ | Sampling time | PPC | Power plant control |
| $RR_{max}$ | Maximum ramp rate | $RR_{min}$ | Minimum ramp rate |
| TSO | Transmission System Operator | FACTS | flexible AC transmission system |
| ESS | Energy storage systems | $\tau_{pv}$ | PV response time |
| $\tau_{bat}$ | battery response time | $C_{bat-nom}$ | Battery nameplate capacity |
| $P_{bat}$ | Battery delivered power | $P^*_{bat}$ | Battery power setpoint |
| $\eta_{bat}$ | Battery efficiency | SOC | Battery state of charge |
| $\alpha$ | PV inverter setpoint | $P_{nom}$ | nameplate plant power |
| $P_{pv}$ | PV power | $P_{pv-av}$ | Available PV power |
| $P_{bat-meas}$ | Measured battery power | $P_{pv-meas}$ | Measured PV power |
| $P_{pcc}$ | Power delivered at the PCC | $P_{pcc-meas}$ | Measured PCC power |
| $\tau_{com}$ | Sending and measurement delay | | |

# Acknowledgements

I would like to thank Edu, my thesis director, for all his guidance and patience during these 5 months working at CITCEA on this thesis. He was available to help me out whenever I encountered difficulties.

I would also like to thank Andreu and Ignacio, who I called many times to get help when I had a problem with the emulation platform, which happened repeatedly. They were very patient with me.

Finally, I would like to thank all the other people in CITCEA, with whom it was nice to work. In particular I would like to thank Monica, who was my teacher during second semester and who introduced me to Edu to do this work, and Oriol Gomis who was my teacher during first semester.

# Chapter 1

# Introduction

Renewable energy sources, such as wind and photovoltaic (PV) power, have an increasing share in the global energy mix. However, the high variability of the available power of these sources implies fast active power fluctuations and can affect grid stability. In this context, the intermittency of renewables has become a critical issue. The operators that manage electrical grids are imposing more and more rules to these plants to ensure that the intermittency of renewables will not affect the stability of the electricity transmission and distribution. As a result, wind and PV power plants have to develop Power Plant Control (PPC) solutions to comply to the rules imposed by grid operators and to ensure proper integration of these plants to the grid.

## 1.1 Objectives

The main objective of this work is to design a PPC solution for hybrid PV-battery power plants, that allows to regulate the power sent by the plant to the grid. This PPC solution is developed under the form of an algorithm that uses the variables measured on the power plant to calculate setpoints that are sent to the the plant afterwards, and this routine is repeated periodically, for instance every second or every 0.2 second. This PPC algorithm is tested on a power plant model developed under Matlab-Simulink, and on a scaled microgrid emulation platform.

## 1.2 Renewable energy sources in electricity production

### 1.2.1 Increasing penetration of renewables in the energy mix

As shown in Figures 1.1 and 1.2, the share of renewable energy sources in electricity production and in the final energy mix (not only electricity) has significantly increased over the past 10 years.

### 1.2.2 Basic facts about photovoltaics

*Since this Master's Thesis is focused on utility-scale PV plants, the aim of this paragraph is to recall the basic knowledge to have about PV.*

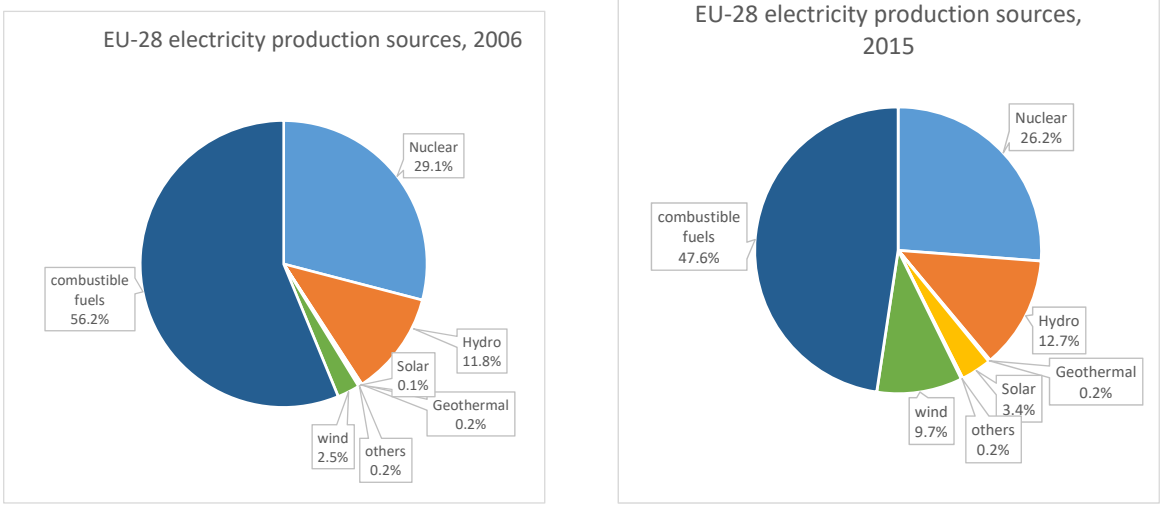


(a) Electricity production sources in the EU-28, 2006 [1]. (b) Electricity production sources in the EU-28, 2015 [1].

Figure 1.1: Evolution of electricity production sources in the EU-28 between 2006 and 2015 [1].

PV is a technology that uses the properties of semiconductor materials to convert solar energy (i.e. photons' energy) into electrical energy. To carry out this conversion, various semiconductor materials may be used. The most widely used are crystalline silicon (c-Si), amorphous silicon (a-Si), III-V materials as InGaP, InGaAs, CdTe, etc. Or more recently, organic materials, silicon nanowires (SiNWs) and perovskites. Figure 1.3 sums up the different PV technologies and their respective record efficiencies throughout the last 40 years.

PV consists of a *direct* conversion of solar energy into electricity, and should not be confused with other applications of solar power, such as *solar thermal* energy (mainly used for domestic hot water), or *concentrated solar power* (CSP), that aims to concentrate a large quantity of solar energy onto a small area, in order to use this heat as a boiler for a classical power plant (Rankine cycle), or to store this heat using molten salts.

The smallest device carrying out the solar energy/electrical energy conversion is called a *solar cell*, and its typical dimension is 10 cm. The typical voltage at the terminals of a solar cell is $\approx 1$ V. Solar cells are then assembled in series, forming a structure called a *PV module*, which typically contains 36, 60 or 72 cells in series. A *PV array* is the structure obtained by assembling several PV modules. A *PV system* is a complete grid-connected electrical system, that generates electricity from solar power. It therefore includes a PV array, but also an inverter to convert the direct current produced by the array into alternative current; a meter, fuses, possibly a battery to store small amounts of energy, and other electrical components can also be involved in a PV system. The relationship between PV cells, modules, arrays and systems is summed up in figure 1.4.

Every manufactured PV module has a nameplate peak DC power $P_0$ (typically 150 – 200 $W_p$) that

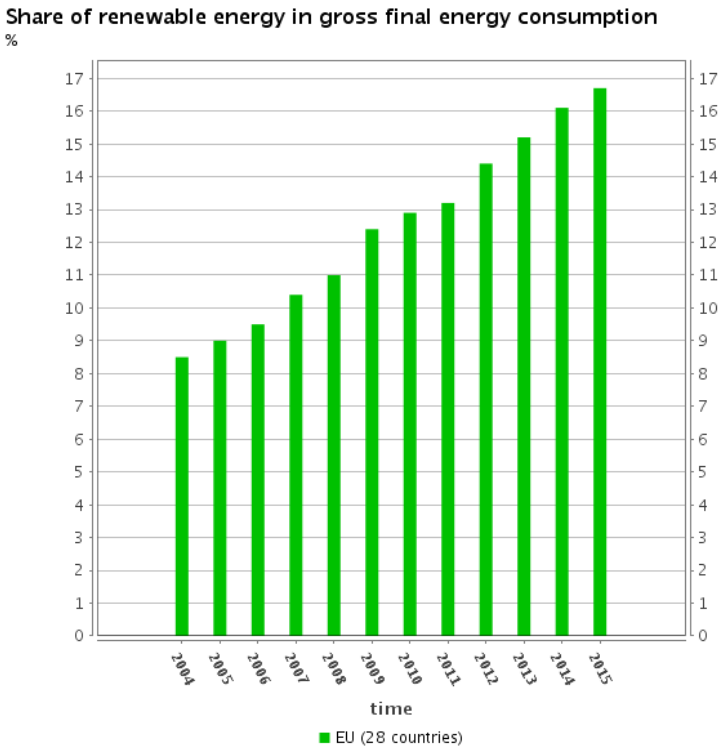


Figure 1.2: Evolution of the share of renewables in the gross final energy consumption, EU-28, 2004-2015 [2].

equals the DC power that would be produced by the module if it was operating at *standard test conditions* (STC), i.e. at a temperature of 25 °C and under a solar irradiance of 1000 W/m$^2$, with a AM 1.5 solar spectrum. However, for grid-connected PV systems, the standard conditions are rarely met since the irradiation is often lower than 1000 W/m$^2$ (and equals 0 during the night), and the air mass can be greater than 1.5 if the sky is cloudy. Therefore, at a given time, the DC power produced by a PV array is most likely lower than its nameplate peak DC power. Moreover, the output AC power produced by the PV system is always lower than the DC power produced by the array, since the DC to AC conversion made by the inverter induces power losses: the typical efficiency of the inverter is $\eta_{inv} = 0.9$.

PV systems can be as small as a dozen of modules (domestic applications with a typical nameplate DC power $P_0 = 1 - 5$ kW$_p$), but can also be much larger, assembled into *PV power plants*. The order of magnitude of the nameplate power of a PV plant is $1 - 100$ MW$_p$. To the date of 2017, there are about 30 PV power plants in the World that have a nameplate power greater than 150 MW$_p$, the biggest having a nameplate power of 850 MW$_p$ (Longyangxia Dam Solar Park, China).

Since the beginning of the 21$^{st}$ century, photovoltaics (PV) has been one of the fastest-growing energy sources. Indeed, as shown in Figure 1.5, the worldwide installed PV capacity has risen from less than 10 GW$_p$ in 2005 to 228 GW$_p$ in 2015. 51 GW$_p$ of PV power capacity have been installed worldwide during the year 2015. [4]

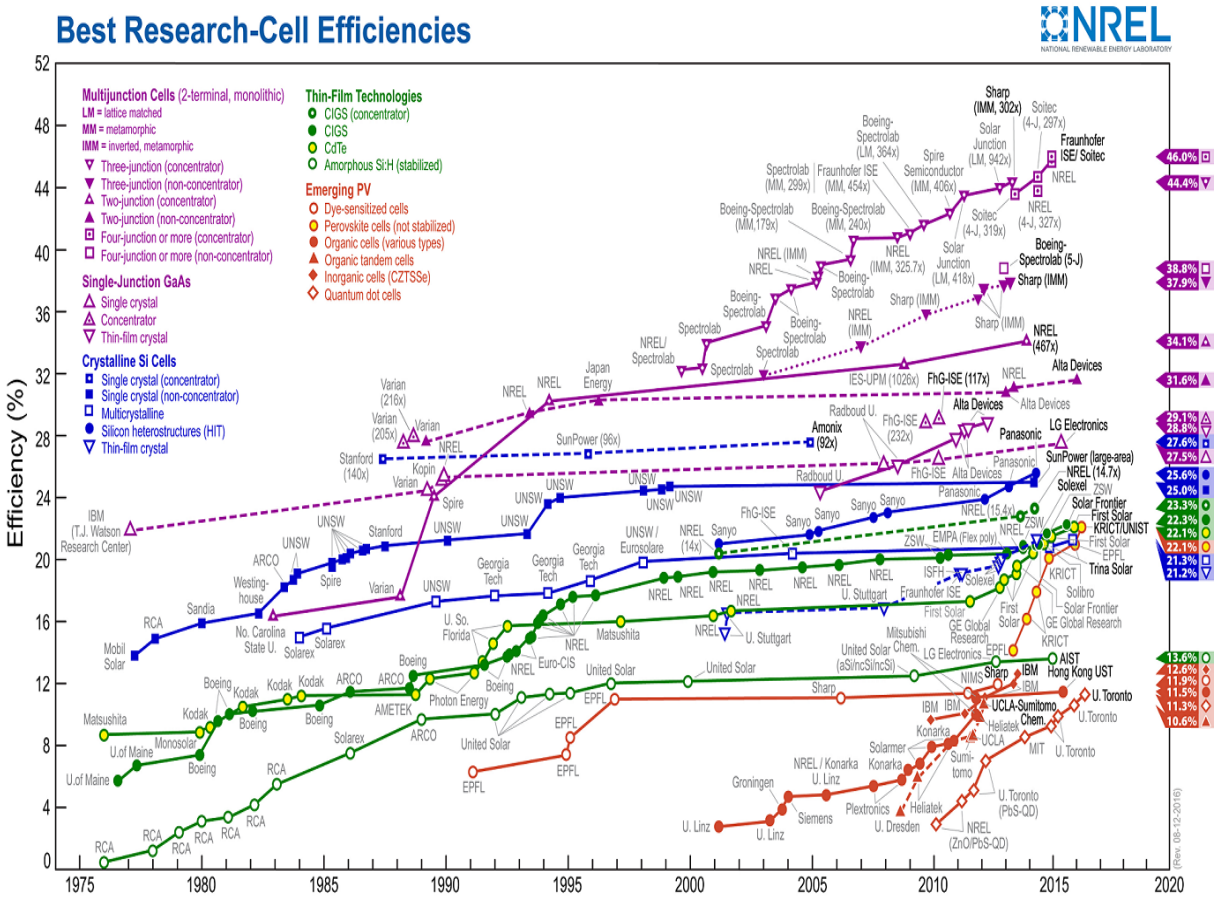


Figure 1.3: Record research-PV cell efficiencies throughout the years, showing the different PV technologies. Source: NREL.

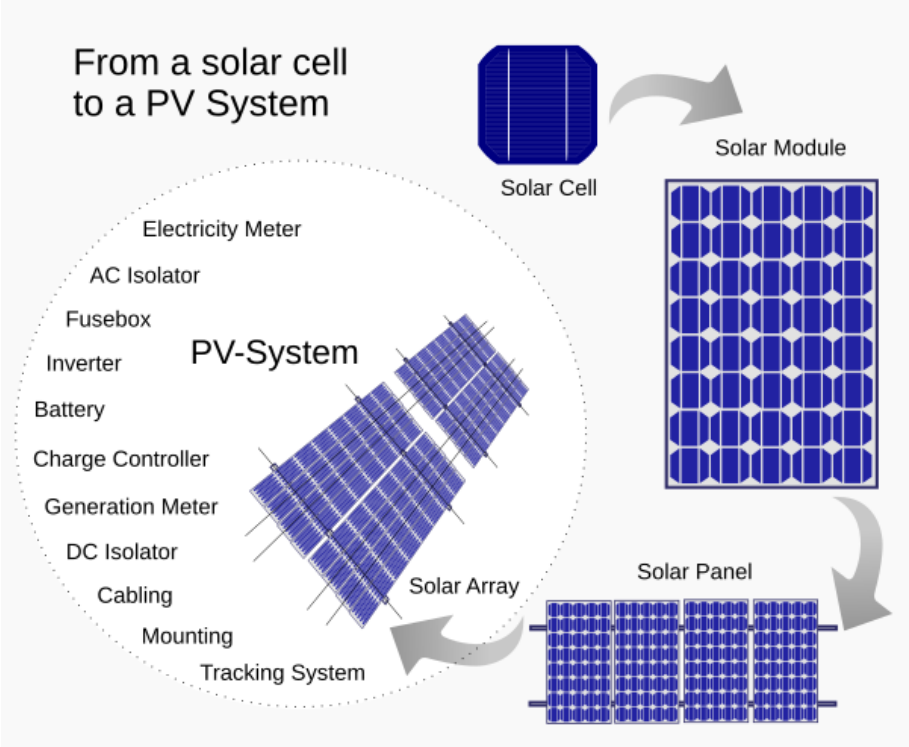


Figure 1.4: PV cell, module array, and system. [3]

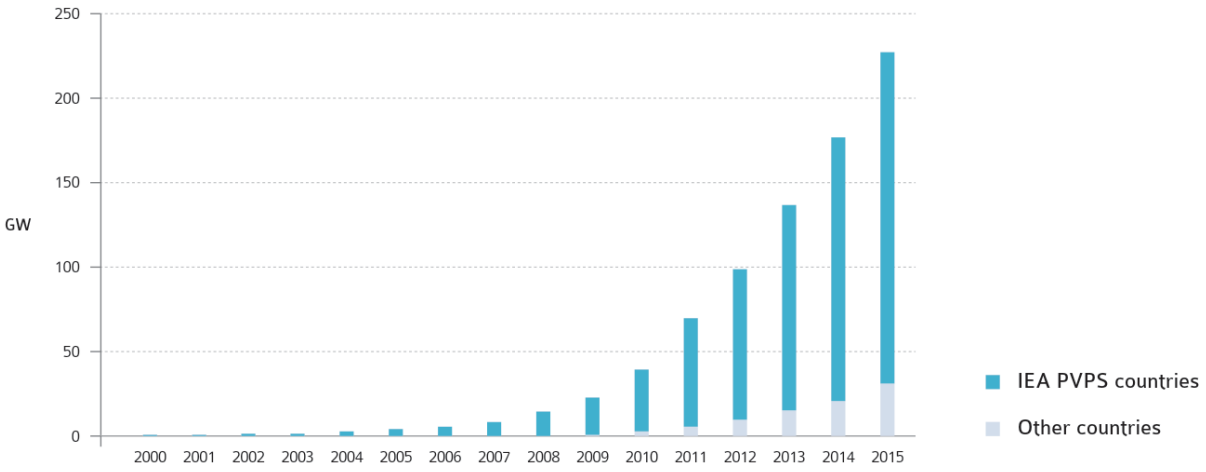


Figure 1.5: Evolution of worldwide installed PV capacity, 2000-2015 [4].

## 1.3 Grid support and grid codes requirements

The general structure of a generic power system is recalled in Figure 1.6. It consists of the following elements:

- Large generation plants, including conventional plants (nuclear, coal, gas, hydro) but also renewable utility-scale plants (wind, PV);
- MV-HV transformers and HV transmission lines to transport the power produced by these plants at high or very high voltages in order to minimize line power losses;
- Substations to support the grid;
- HV-MV and MV-LV transformers to step down the voltage for consumer distribution, as well as MV and LV distribution lines;
- Distributed generation such as home-scale PV systems.

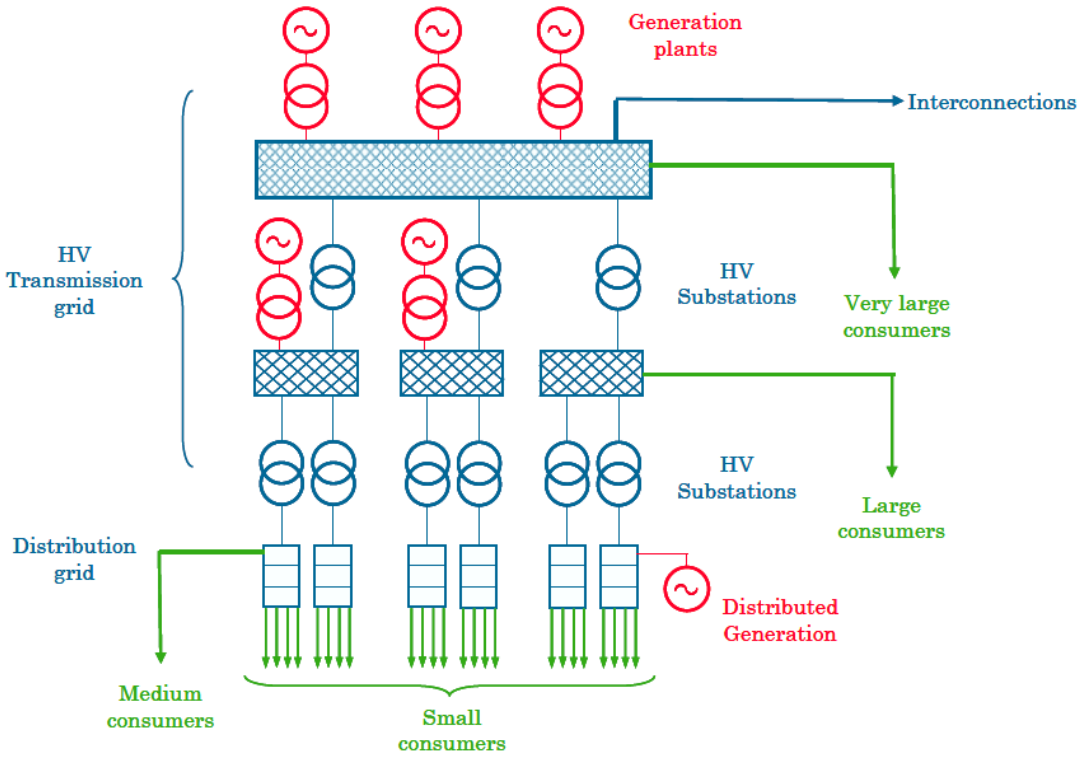


Figure 1.6: Power system structure [5].

### 1.3.1 Grid codes

The critical issues in a power system are:

- to deliver a power matching the demand of the grid;
- to regulate the grid frequency (the intrisic relationship between these two first points will be specified below);
- and to control voltage in order to avoid voltage drops that would prevent from transmitting the proper quantity of active power to the loads.

To achieve these goals, Transmission System Operators (TSOs) have set up *grid codes* that impose technical requirements to the plants. Fulfilling these technical requirements allows the grid to be stable, secure and reactive in case of any power event, frequency event or unexpected disconnection of a load/a generation unit. This framework is called *grid support*.

### 1.3.2 Frequency regulation

Conventional (such as nuclear, coal or gas) power plants operate by transforming the fuel heat into mechanical work, specifically under the form of the kinetic rotational energy of a turbine. This kinetic energy is then use to produce electricity through the use of a synchronous machine (generator). The rotational speed $\omega$ of the generator satisfies the following equation:

$$\frac{J\omega}{p}\frac{d\omega}{dt} = P_m - P_e \tag{1.1}$$

where:

- $J$ is the inertia of the machine;
- $p$ is the number of poles of the machine;
- $P_e$ is the electrical power;
- $P_m$ is the mechanical power provided by the turbine.

In steady state the synchronous machines providing power to the grid are rotating at the same frequency than the grid nameplate frequency ($f = 50$ Hz in most of the countries, $f = 60$ Hz in some others), $\omega$ remains constant and as a consequence of equation 1.1, the mechanical power $P_m$ exactly cancels out the slow-down implied by the load electrical consumption $P_e$.

However, if the load increases (demand + losses > production), $P_e$ will become greater than $P_m$ and as a consequence of equation 1.1 the rotational speed of the synchronous machines connected to the grid will decrease, therefore decreasing the global frequency of the current delivered to the grid. For the grid to retrieve its normal frequency, more power should be produced (or the load should be diminished, if possible).

Conversely, if the load decreases (demand + losses < production), $P_e$ will become smaller than $P_m$ and as a consequence of equation 1.1 the synchronous machines will start to accelerate, therefore increasing

the global frequency of the current delivered to the grid. For the grid to retrieve its normal frequency, less power should be produced, if possible.

All of the above can be summed in the following sentence: *frequency is regulated with active power*. Grid codes typically define an *active power setpoint* as a function of frequency. The curves of the active power setpoint as a function of the frequency, for several grid codes, are shown in Figure 1.7. Note that the power setpoint for the normal frequency, denoted as $P_1$, is lower than the available power $P_{available}$ in order to be able to increase the power in case of down-frequency event.

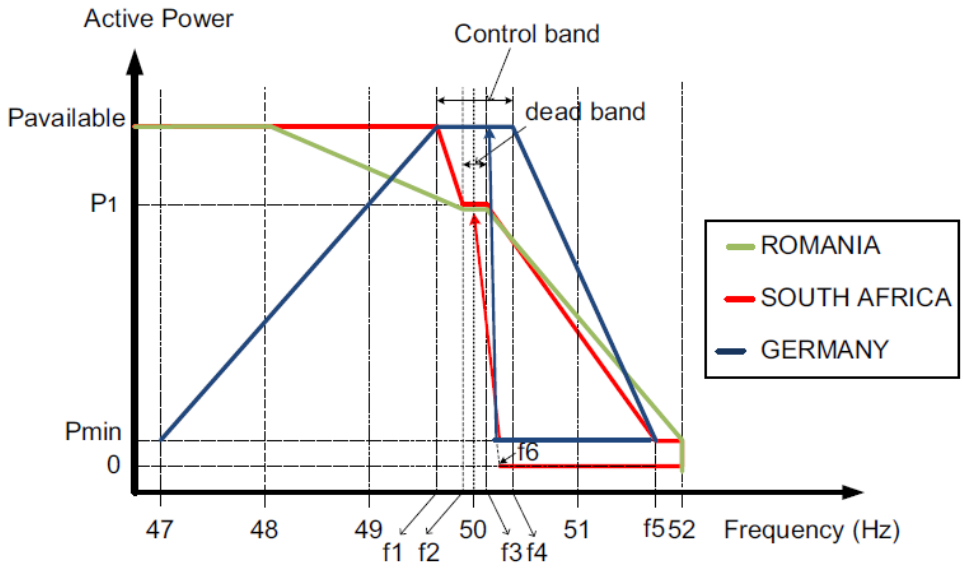


Figure 1.7: Active power setpoints for frequency regulation in several grid codes [6].

### 1.3.3 Voltage regulation

Similarly to frequency that can be regulated by injecting or absorbing active power, voltage can be regulated by injecting or absorbing reactive power.

A low voltage fault-ride through (LVFRT) is the ability of a plant to stay connected to the grid during an event of abnormally low voltage. Grid codes specify, for low-voltage faults, the minimum time during which the plant must remain connected to provide grid support. These requirements are presented in Figure 1.8 for several grid codes.

### 1.3.4 Active power regulation

As discussed above, the active power is used to regulate grid frequency. But the active power itself also has to be regulated, following several criteria:

- Active power reserve (or delta constraint);

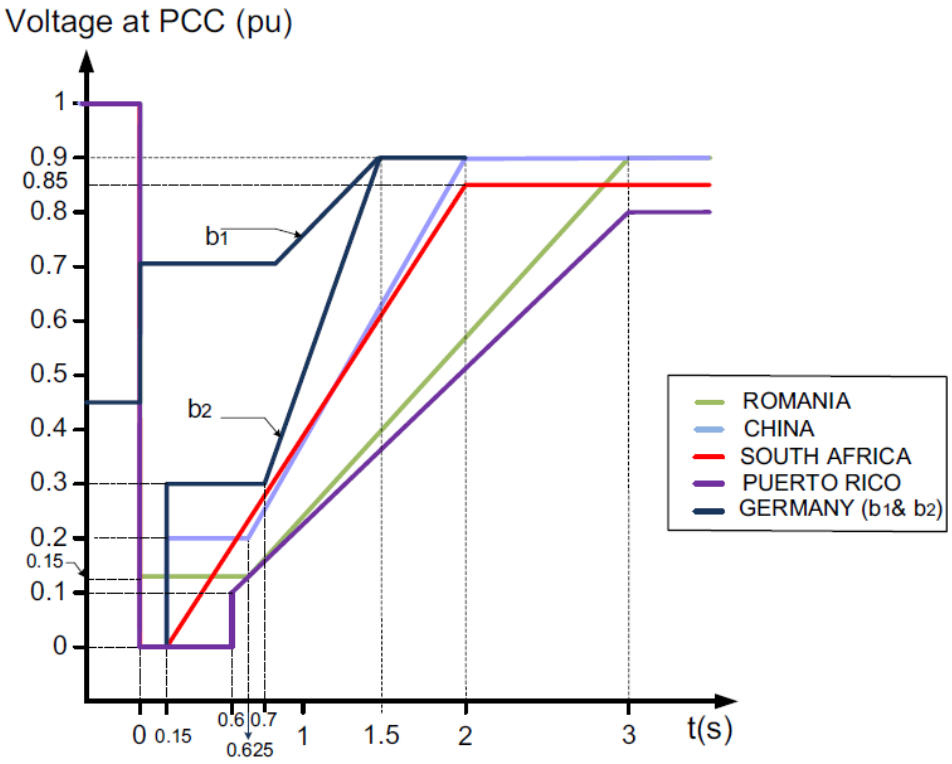


Figure 1.8: Comparison of LVFRT requirements in several grid codes [6].

- Absolute active power setpoint (that is not necessarily equal to the total available power; if it is not the case, the situation is called a *power curtailment*);
- Ramp rate limitation, which means that active power variations cannot exceed a fixed rate, for instance 10% of the plant nameplate power per minute.

Figure 1.9 illustrates these constraints that can applied on active power.

For instance, for Hawaii's grid code the ramp rate is evaluated by comparing the power delivered to the grid at time $t$ with the power delivered at time $t-5$ s. For the grid code of Porto rico, there is a recommendation of evaluating the ramp rate over time intervals of 2 seconds.

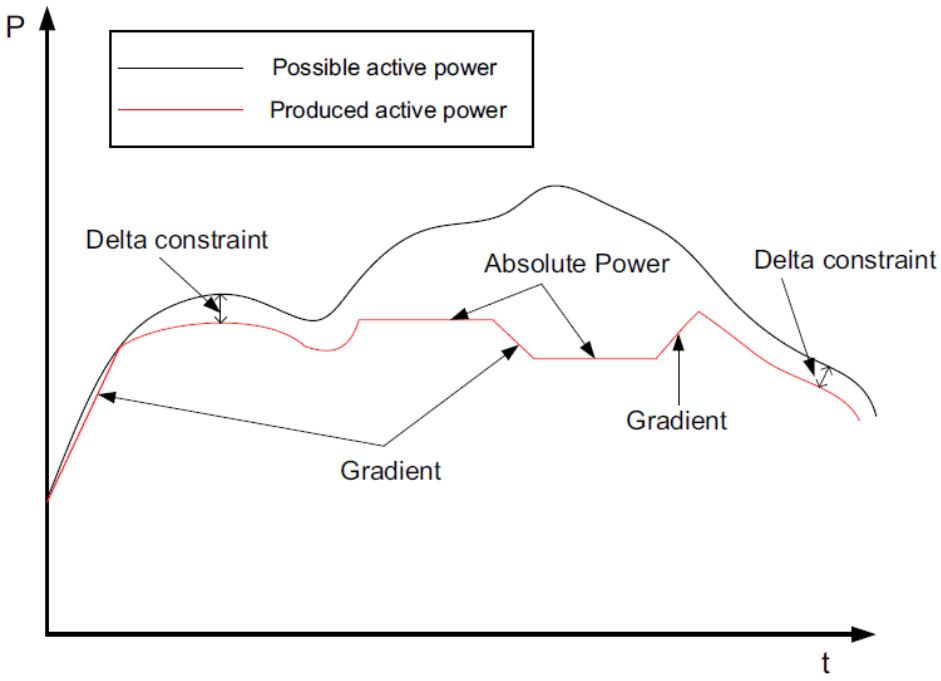


Figure 1.9: Illustration of the various constraints on active power [6].

## 1.4 Necessity of a Power Plant Control solution

The increasing share of renewables in the energy mix (see paragraph 1.2.1) has lead TSOs to make renewable plants participate in grid support (see section 1.3). As a result, grid code requirements have become increasingly demanding with renewable sources power plants [7, 8, 9, 10]. To fulfill these requirements, wind and PV plants must be provided with proper devices (e.g. FACTS devices, capacitor banks) that should be managed by a power plant control (PPC) solution.

### 1.4.1 Principle of a power plant controller

A PPC solution relies on the following elements:

- regular measurements of the variables of the power plant (every second or even every 0.2 second);
- in certain cases, use of meteorological forecasts to anticipate changes of the plant variables (but it will not be the case in this work);
- use of algorithms to calculate orders (synonym: *setpoints*) to be sent to the different devices of the plant;
- communication infrastructure to receive the measurements and deliver the setpoints.

### 1.4.2 State of the art

In [11], a PPC algorithm for large-scale PV plants is presented, tested on-site on a 9.4 MW PV plant in Romania (Vanju-Mare PV plant) and validated. This controller relies on the use of devices such as FACTS devices and capacitor banks to manage active and reactive power of the PV plant. However, this controller does not take account of energy storage systems (ESS) such as batteries.

In [12], the PPC algorithm developed in [11] is improved to be used in a hybrid PV-ESS power plant. This PPC solution proposes a direct ramp rate limitation, as opposed to other solutions in literature that relates on traditional filtering or moving-average techniques. This thesis proposes a validation of this PPC algorithm on a scaled platform that emulates a hybrid PV-battery power plant.

# Chapter 2

# Plant model and control design

In this chapter, it is presented a PPC strategy in order to control the active power ramp rate limitations of the hybrid PV-battery power plant. To do so, the battery is controlled so that it generates or absorbs the lack/excess of energy production. In addition, a state of charge control is performed to ensure the battery always has enough capacity to perform its operation. This PPC algorithm is, with minor changes, the one presented in [12].

## 2.1 Hybrid PV/battery power plant model

### 2.1.1 Plant model

Figure 2.1 shows a general scheme of a hybrid battery/PV power plant with a Power Plant Controller (PPC). Typically, three-winding transformers interconnect the PV arrays to the internal PV power plant grid. The battery and its associated inverter are also connected to the plant internal grid by a transformer. The internal grid is interconnected to the transmission grid through a MV/HV transformer. The grid code requirements are set at the interconnection point with the HV grid, also called Point of Common Coupling (PCC). Therefore, in the framework of the power plant control, the power that needs to be controlled and to comply with the grid code requirements is the power at the PCC, noted $P_{pcc}(t)$. For the battery control, the battery power and its state of charge are measured at the output of the battery. The Power Plant Controller also sends setpoints to the battery and the PV inverters.

The block diagram of the plant model is shown in figure 2.2. The model includes a battery model, and an equivalent PV power generator that represents the PV arrays and the PV inverters. It takes into account the sending and measurement delays, with a communication delay $\tau_{com}$. The measured SOC, battery power, PCC power and PV power are sent to the PPC that sents the appropriate setpoints to the battery and the PV generator.

### 2.1.2 Battery model

The battery model is shown in figure 2.3. $P_{bat}$ denotes the power generated by the battery. It is positive if the battery is delivering power, and negative if the battery is absorbing power. $P^*_{bat}$ is the setpoint sent to the battery. $C_{bat-nom}$ [kWh] is the nameplate capacity of the battery, and $\eta_{bat}$ its efficiency. The dynamics

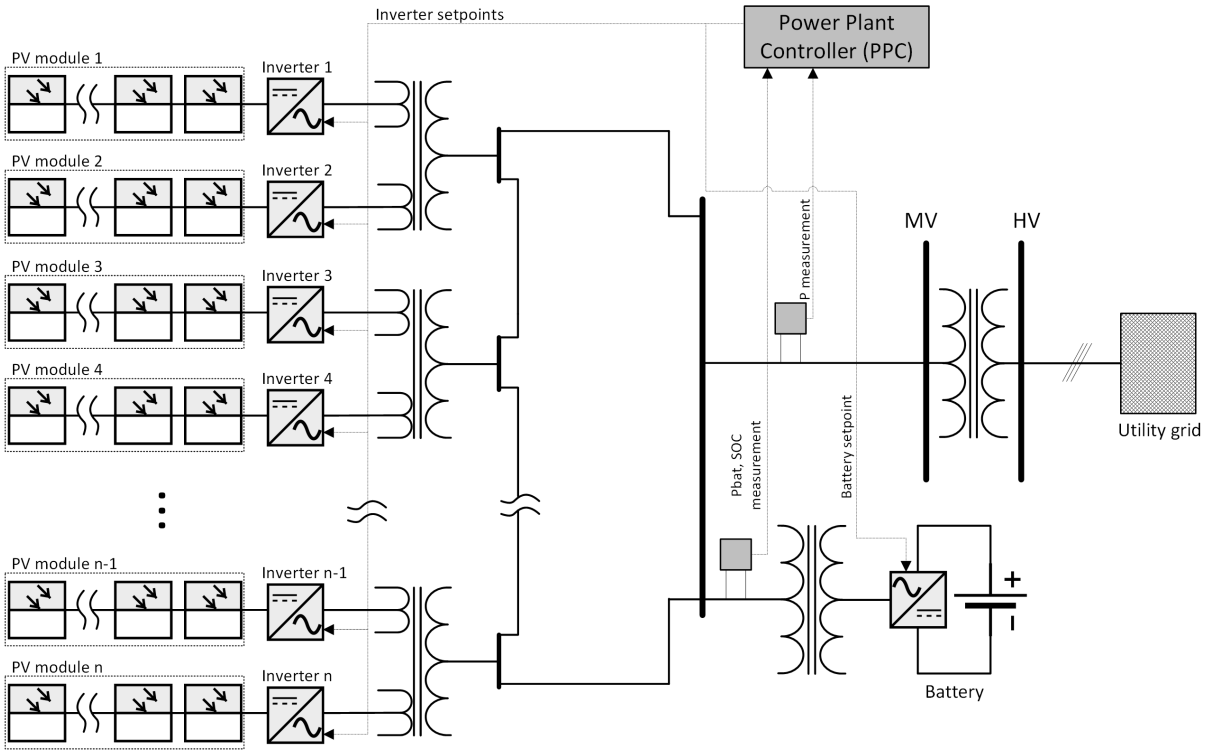


Figure 2.1: Scheme of a hybrid battery/PV plant.

of the battery and its associated inverter can be modeled as a first-order function $\frac{1}{1+\tau_{bat}s}$ [13]. Moreover, the power delivered or absorbed by the battery cannot exceed given values $P_{bat-max}$ and $P_{bat-min}$. The state of charge (SOC) of the battery, which is a normalized value between 0 and 1, is calculated by integrating $P_{bat}(t)$ (taking account of the battery efficiency) and dividing it by the nameplate capacity. The definition of SOC implies:

$$P_{bat-max} = \begin{cases} P_{bat-nom} & \text{if } SOC > 0 \\ 0 & \text{if } SOC = 0 \text{ (empty battery)} \end{cases} \tag{2.1}$$

$$P_{bat-min} = \begin{cases} -P_{bat-nom} & \text{if } SOC < 1 \\ 0 & \text{if } SOC = 1 \text{ (full battery)} \end{cases} \tag{2.2}$$

where $P_{bat-nom}$ is the nameplate capacity of the battery.

### 2.1.3 PV generator model

The PV generator (PV arrays and inverters) model is shown in figure 2.4. It is an *aggregated* model, as all the PV modules and their associated inverters are modeled by a single generator.

If $P_{plant}$ is the nameplate power of the plant and $P_{tot}$ the active power setpoint, $\alpha = \frac{P_{tot}}{P_{plant}}$ is the per unit setpoint. This single setpoint $\alpha$ will be sent to each inverter, and the power setpoint for the inverter $i$ will then be given by $P^*_{pv,i} = \alpha P_{nom,i}$, where $P_{nom,i}$ denotes the nameplate power of the inverter $i$. The

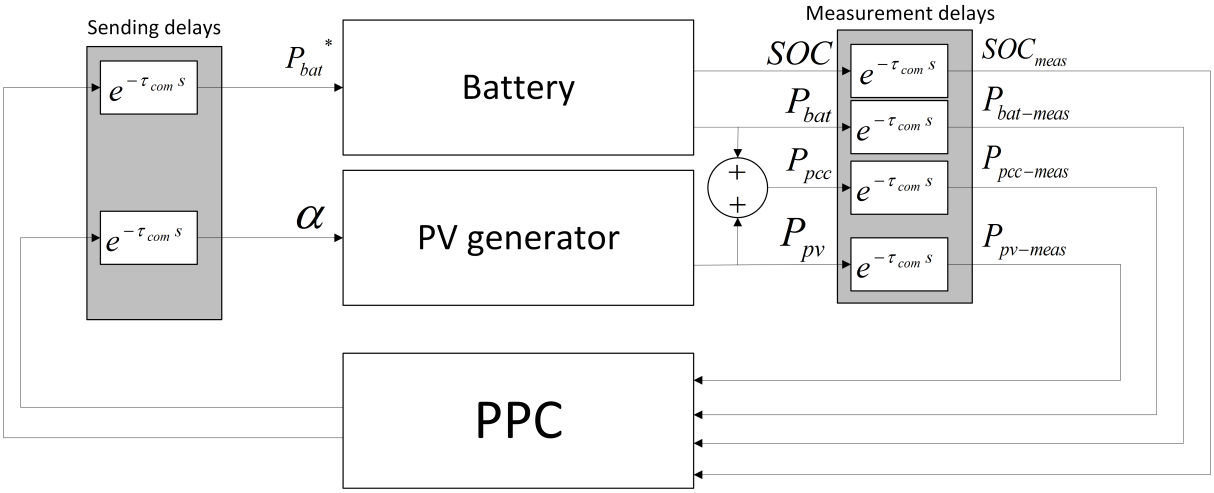


Figure 2.2: Hybrid battery/PV plant model.

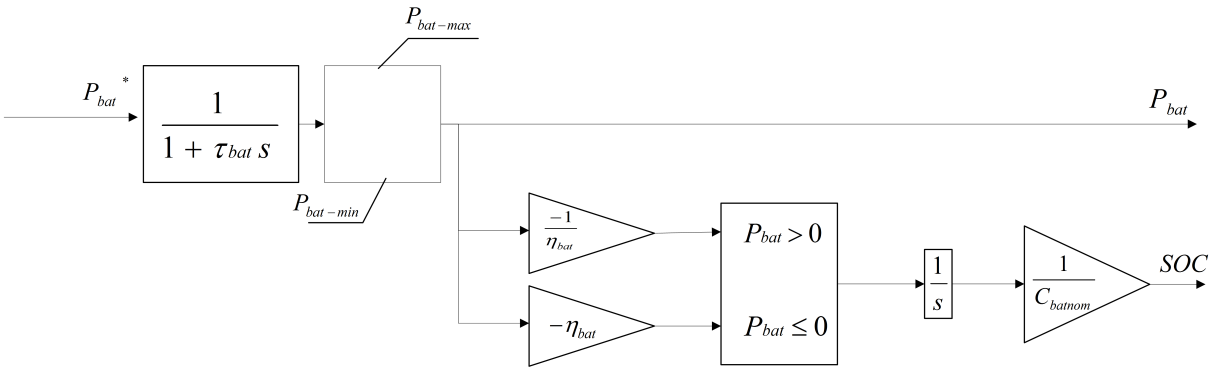


Figure 2.3: Battery model.

dynamics of this equivalent PV generator can be modeled by a first-order function $\frac{1}{1+\tau_{pv}s}$. The PV power $P_{pv}$ is saturated by the available PV power $P_{pv-av}$.

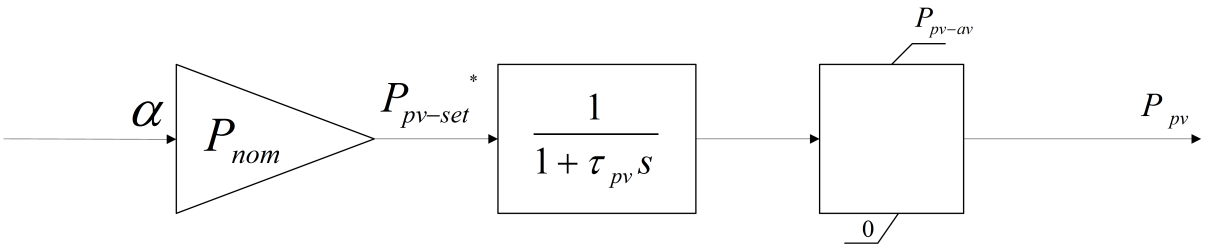


Figure 2.4: PV generator model.

## 2.2 Ramp rate controller

### 2.2.1 Justification

Some grid codes [9] require PV plants to limit by a ramp rate the variations of the power delivered by the plant to the grid at the point of common coupling (PCC), $P_{pcc}(t)$. The controller presented in this work allows a direct control of the ramp rate, oion contrast to mainly used techniques to soften the variations of $P_{pcc}(t)$, such as filtering or moving averages. Indeed, the advantage of a direct ramp rate control is that the battery operates only when it is strictly necessary, and as a result the battery energy flow is reduced in comparison to other control strategies [12].

### 2.2.2 Description and presentation

The time window $T_w$ used in the ramp rate control is usually imposed by the TSO. The value $T_w = 2$ s will be taken in the rest of this thesis. The principle of the ramp rate controller is the following: Every sampling time $T_s$, the values of $P_{pv}(t)$ and $P_{pcc}(t - T_w)$ are compared.

- If the PV power $P_{pv}$ increases too fast, the battery will absorb the excess of power ($P_{bat} < 0$) so that $P_{pcc}(t)$ complies to the maximum ramp rate.
- Conversely, if the PV power $P_{pv}$ decreases too fast, the battery will deliver the lack of power ($P_{bat} > 0$) so that $P_{pcc}(t)$ complies to the minimum ramp rate.
- If the power variation $P_{pv}(t) - P_{pcc}(t - T_w)$ is within the ramp rate limitation, the battery will not be solicited ($P_{bat} = 0$).

This principle is summed up in Figure 2.5.
The equations that define the next battery setpoint, according to this principle, are given by:

$$P^*_{bat}(t) = \begin{cases} \Delta P_{min} + P_{pcc}(t - T_w) - P_{pv}(t) & \text{if } P_{pv}(t) - P_{pcc}(t - T_w) < \Delta P_{min} \\ \Delta P_{max} + P_{pcc}(t - T_w) - P_{pv}(t) & \text{if } P_{pv}(t) - P_{pcc}(t - T_w) > \Delta P_{max} \\ 0 & \text{otherwise} \end{cases} \tag{2.3}$$

In these expressions, $\Delta P_{min}$ and $\Delta P_{max}$ are respectively the minimum and the maximum allowed power variation over a time $T_w$. They can be expressed as:

$$\Delta P_{min} = \frac{RR_{min}}{100} P_{plant} \frac{T_w}{60} \tag{2.4}$$

$$\Delta P_{max} = \frac{RR_{max}}{100} P_{plant} \frac{T_w}{60} \tag{2.5}$$

where $RR_{min}$ and $RR_{max}$ are expressed as percentages per minute, e.g. $RR_{min} = -10\%/\text{min}$ and $RR_{max} = -10\%/\text{min}$. $\frac{T_w}{60}$ is the value of $T_w$ in minutes. These limit ramp rates mean that the power cannot increase (or decrease) faster than 10% of the nameplate power plant every minute. With $P_{plant} = 9.4\text{MW}$ (Vanju-Mare PV plant) and $T_w = 2$ s we find $\Delta P_{min} = -31.33$ kW, $\Delta P_{max} = 31.33$ kW.

### 2.2.3 Illustration of the effect of the ramp rate limitation

*Note that in this paragraph, the plant model used is an ideal one and not the model previously presented in this chapter: in particular, the battery is "infinite" (there is no maximum nor minimum battery power, and the capacity is not limited), and the dynamics of the various plant elements are not taken into account. The results with the whole plant model will be presented in Chapters 3 (simulations with Simulink) and 4 (emulation on the scaled microgrid platform).*

The aim of this paragraph is to illustrate on a simple example the principle of the ramp rate limitation. The next figures present the results of the ramp rate limitation over a given PV profile. This PV power profile has a sampling time of 1 second and lasts for 2000 seconds (approximately 34 minutes). As it corresponds to a morning with high meteorological variability, the PV power profile presents rapid variations.

Figure 2.6 presents the PV power profile $P_{pv-available}(t)$ (blue line) along with the results of the ramp rate limitation, namely the battery power $P_{bat}(t)$ (cyan line) and the power injected into the grid $P_{pcc}(t)$ (red line). The sampling time is $T_s = 1$ s and the "time window" $T_w$ defined in equations 2.3 is $T_w = 2$ s. The plant nameplate power is $P_{plant} = 9400$ kW, and the ramp rate limit is 10%/minute of the plant power, that is, a maximum variation of 940 kW/min, or 31.33 kW over every interval of 2 seconds.

For more clarity, figure 2.7 shows the quantity (blue line) $P_{pv}(t) - P_{pcc}(t - T_w)$ that is compared to $\Delta P_{min}$ and to $\Delta P_{max}$ to carry out the ramp rate limitation. The critical values are represented with dashed horizontal red lines. When this quantity is greater than $\Delta P_{max}$ this is a "ramp-up" event and the battery will absorb power; conversely, when this quantity is lower than $\Delta P_{min}$ this is a "ramp-down" event and the battery will provide power.

Another way of quantifying the changes implied by the ramp rate limitation is to plot the evolution of the ramp rate over time, and its statistical distribution, before and after the application of the ramp rate limitation. The results are presented in Figure 2.8. Clearly, over the chosen sample, the PV power has variations exceeding the limit during a non-negligible part of the experience. The "natural" ramp rate calculated with $P_{pv}(t) - P_{pv}(t - T_w)$ exceeds the limits of $\pm 10\%/\text{min}$ a lot a times, as it can be observed on the histogram in Figure 2.8b.

Conversely, after application of the ramp rate limitation, the ramp rate always lie between the chosen limits $\pm 10\%/\text{min}$, and as it can be observed on the histogram in Figure 2.8d, most of the excessively high ramp rates have been brought down to $+10\%/\text{min}$, and similarly the excessively low ramp rates have been brought up to $-10\%/\text{min}$. Looking back at Figure 2.6 one can clearly see during which periods of time the ramp rate was equal to its extreme values.

Note that this is an ideal case, because the battery dynamics are not taken into account, and neither are the sending and measurement delays. This was just to illustrate the idea of ramp rate limitation. More realistic simulations will be carried out later in this work.

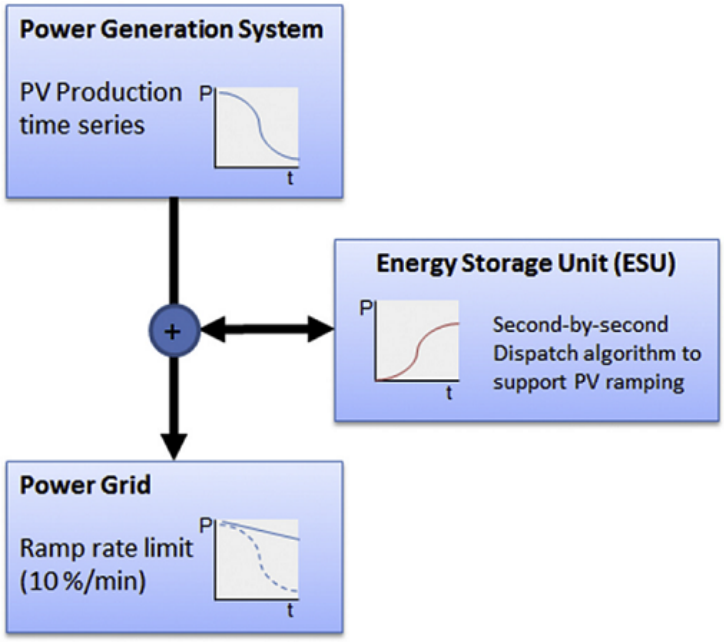


(a) Illustrated principle of the ramp rate control [14].

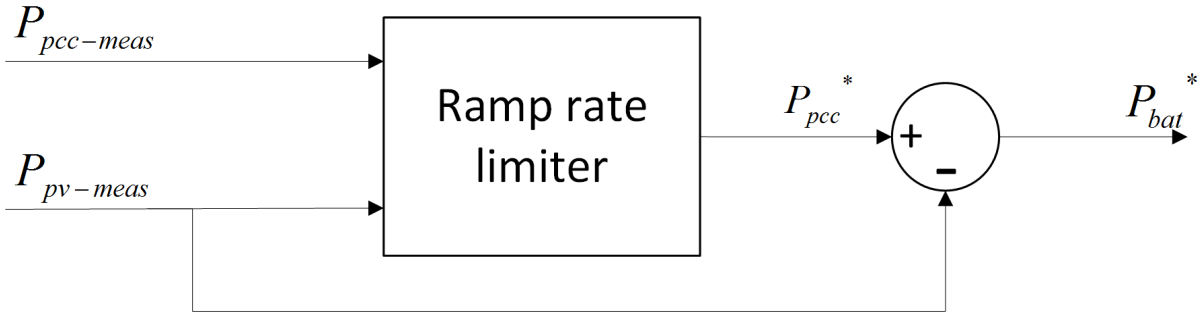


(b) Block diagram of the ramp rate controller.

Figure 2.5: Principle of the ramp rate limitation on $P_{pcc}(t)$.

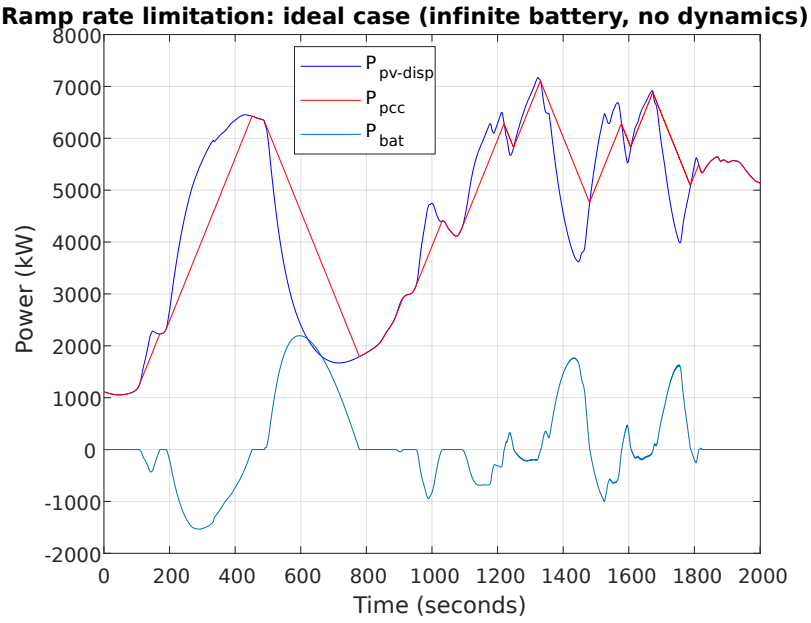


Figure 2.6: Effect of a ramp rate limitation of 10%/minute of the nameplate plant power. In this case $P_{plant} = 9400$ kW therefore the limit ramp rate is 940 kW/min.

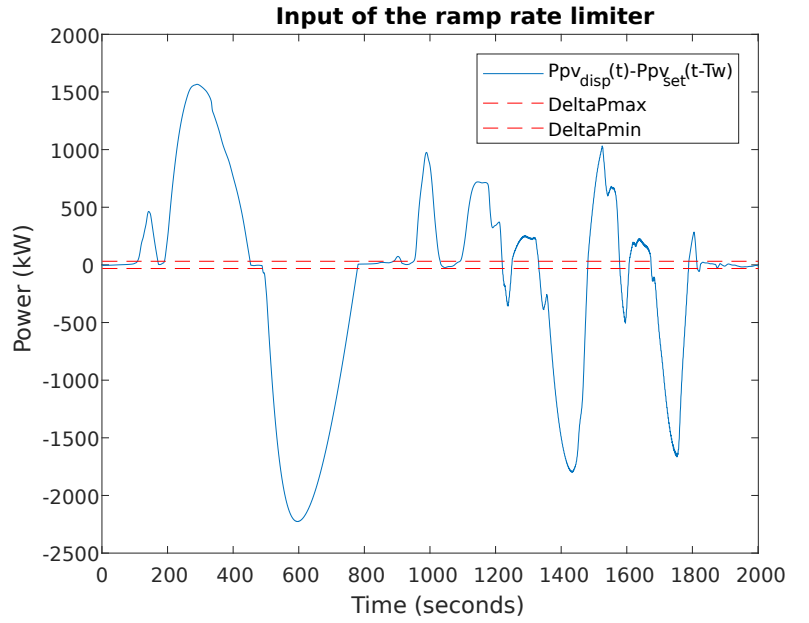


Figure 2.7: Plot of the quantity $P_{pv}(t) - P_{pcc}(t - T_w)$ that is evaluated to carry out the ramp rate limitation. The red lines indicate the limit values $\Delta P_{max}$ and $\Delta P_{min}$.

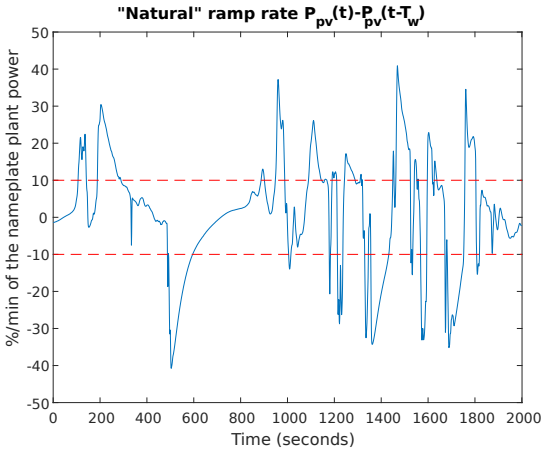


(a) "Natural" ramp rate calculated from the PV profile.

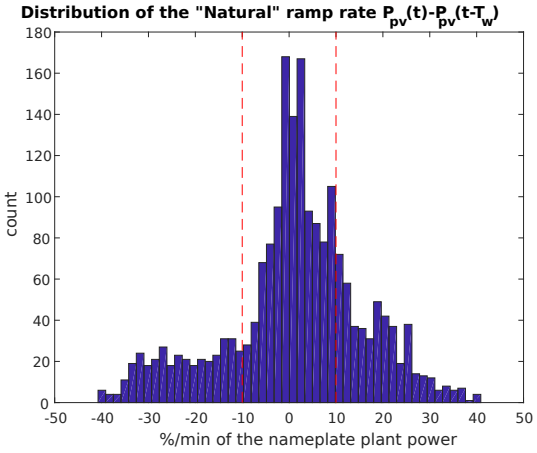


(b) Distribution of the "natural" ramp rate.

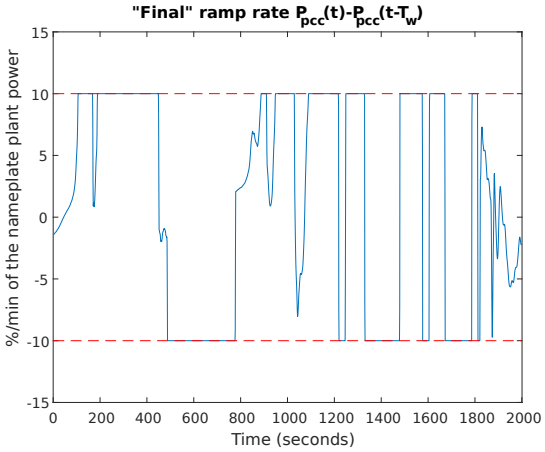


(c) "Final" ramp rate after application of the ramp rate limitation.

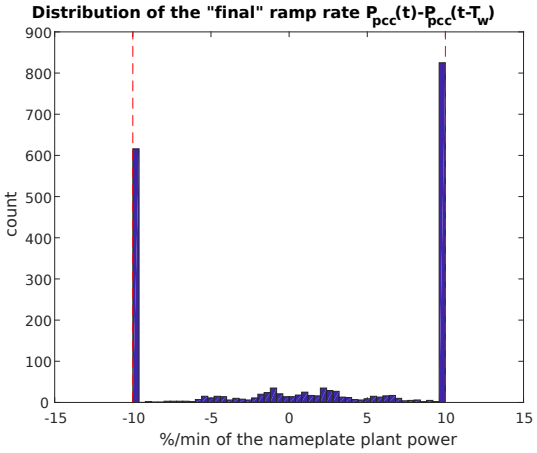


(d) Distribution of the "final" ramp rate.

Figure 2.8: Comparison of the ramp rates (evolution with time, and statistical distribution) without the ramp rate limitation (2.8a, 2.8b) and with the ramp rate limitation (2.8c, 2.8d).

## 2.3 SOC control

### Justification

Energy storage systems such as flywheels and supercapacitors have a long cycle-life (typically 100 000 cycles) and a relatively high Power:Energy ratio, i.e. the speed at which they absorb or release energy is relatively high in regard to their energy capacity. Therefore, systems such as flywheels and supercapacitors perform fast charge/discharge cycles, and their state of charge (SOC) will often be close to 0 or to 100%.
Conversely, batteries have a lower Power:Energy ratio and a lower cycle-life. Therefore, to maximize its life duration, it is a better strategy not to perform entire cycles with a battery and to make it operate most of the time at a SOC between 40% and 60% [14].

### Description and presentation

As written above, to preserve the lifespan of the battery it is preferable to make it operate with a SOC around 50% at all time, typically between 0.4 and 0.6. In this paragraph is defined a setpoint that fulfills this condition. If the PV power is high, ramp-down events are more likely to occur, and therefore it is likely that the battery will be solicited to inject power into the grid ($P_{bat} > 0$). Therefore the SOC should be high when the PV power is high, so that the battery can inject power. Conversely, the SOC should be low when the PV power is low, so that the battery can absorb power ($P_{bat} < 0$) during ramp-up events. The SOC setpoint will be defined by a simple linear function:

$$SOC^*(t) = 0.4 + \frac{(0.6-0.4)P_{pv}(t)}{P_{plant}} \tag{2.6}$$

The ramp rate control on $P_{bat}(t)$ presented in section 2.2 is improved in order to control the SOC. To do so, a proportional corrector is used, calculating an error $e(t)$:

$$e(t) = K_{SOC}(SOC(t) - SOC^*(t)) \tag{2.7}$$

This error is the difference between the actual (measured) SOC and the SOC setpoint, that was defined above, multiplied by a gain $K_{SOC}$. The smaller the value of the gain $K_{SOC}$, the smaller is the influence of the proportional controller. It means that if $K_{SOC}$ is too small, the SOC will not be effectively bounded in the interval 0.4-0.6 as requested. Conversely, if $K_{SOC}$ is very high, the SOC will be easily bounded in the interval 0.4-0.6, but it will also imply that the error $e(t)$ will be larger, affecting the input of the ramp rate limiter and therefore affecting the effectiveness of the ramp rate limitation. As a result, several values of $K_{SOC}$ should be tried in order to tune the proportional controller and find a good equilibrium between effectively bounding the SOC to the interval 0.4-0.6 on one hand, and not perturbate the ramp rate limitation too much on the other hand. Figure 2.9 shows the modified block diagram of the control, including this proportional controller.

Equations 2.3 are then modified into:

$$P^*_{bat}(t) = \begin{cases} \Delta P_{min} + P_{pcc}(t-T_w) - P_{pv}(t) & \text{if } P_{pv}(t) - P_{pcc}(t-T_w) - e(t) < \Delta P_{min} \\ \Delta P_{max} + P_{pcc}(t-T_w) - P_{pv}(t) & \text{if } P_{pv}(t) - P_{pcc}(t-T_w) - e(t) > \Delta P_{max} \\ -e(t) & \text{otherwise} \end{cases} \tag{2.8}$$

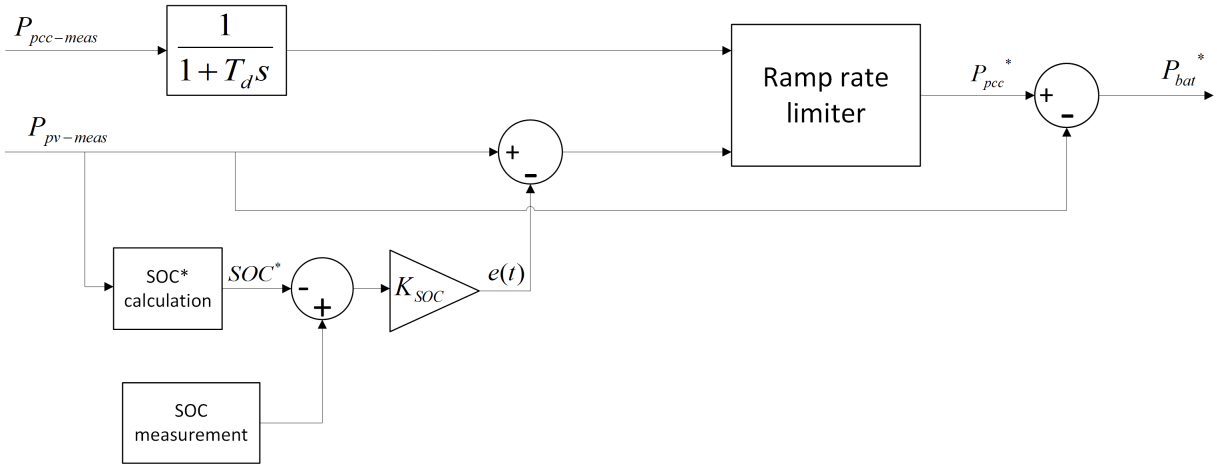


Figure 2.9: Principle of the control, with a filter on $P_{pcc-meas}(t)$ and a proportional controller on the SOC.

# Chapter 3

# Simulations with Simulink

Before starting to carry out emulations on the emulation platform, a necessary step was to test the plant model and the PPC algorithm using a dynamic simulation software. The software chosen to do so was Simulink.

Simulink is a block diagram environment for multidomain simulation and Model-Based Design. It supports simulation, automatic code generation, and continuous test and verification of embedded systems. Simulink provides a graphical editor, customizable block libraries, and solvers for modeling and simulating dynamic systems. It is integrated with MATLAB, allowing to incorporate MATLAB algorithms into models and export simulation results to MATLAB for further analysis [15].

## 3.1 Response to a step event

The aim of the ramp rate limitation is to soften the rapid variations of PV power. Therefore, in this section is studied the response of the ramp rate limiter to a very fast variation of PV power. A typical sudden event can be modeled by a step function.

### 3.1.1 Methodology

Initially, the battery has a state of charge $SOC = 0.5$, and the PV power is constant $P_{pv} = 6$ MW. At $t_0 = 299.8$ s, the available PV power goes instantly down from 6 MW to 5.5 MW (step profile) The value of $t_0$ was chosen high enough to avoid any initialization issue, and such that the step does not occur at a sampling time. The measurement delays and the control sending delays are $\tau_{com} = 20$ ms.
For the data to be properly measured, the time window $T_w$ must be an integer multiple of $T_s$, i.e. $T_w = nT_s$ with $n$ a positive integer.

In this event, the power $P_{PCC}$ has to decrease from 6000 to 5500kW. Therefore, if it decreases at the minimum ramp rate rate $RR_{min} = -10\%/\text{min}$, the duration of the ramp-down event should be equal to:

$$T_{ramp} \approx \frac{(5500-6000)T_w}{\Delta P_{min}} = 31.91 \text{ s} \tag{3.1}$$

### 3.1.2 Influence of the sampling time $T_s$

First will be studied the influence of the ratio $n = T_w/T_s$, without changing the dynamics of the battery (characteristic time $\tau_{bat} = 0.100s$).

Simulation 1 : $n = 1$, $T_w = T_s = 2s$. The results are presented in Figure 3.1 (blue solid line: PV power; red solid line: power measured at the PCC; green dashed line: power measured at the PCC 2 seconds before; blue dashed line: ramp rate limitation).

**Simulation 1**

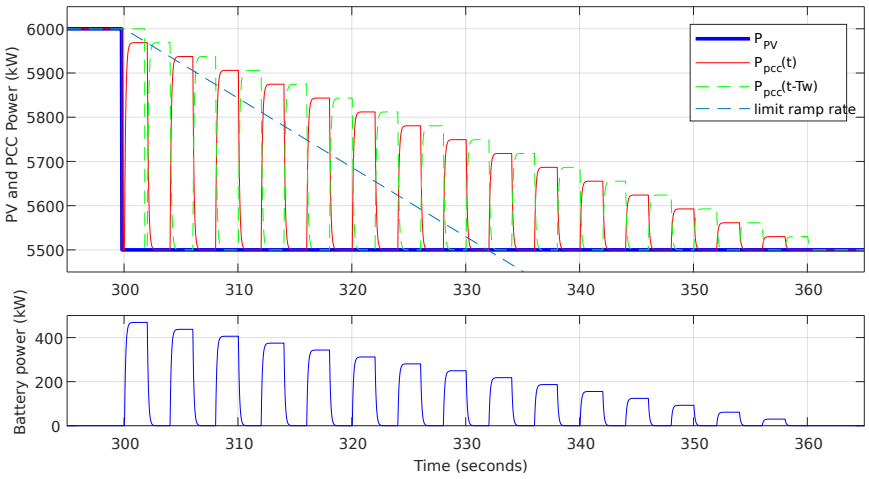


(a) Results of simulation 1: PV power and power delivered at the PCC (top) and power delivered by the battery (bottom).

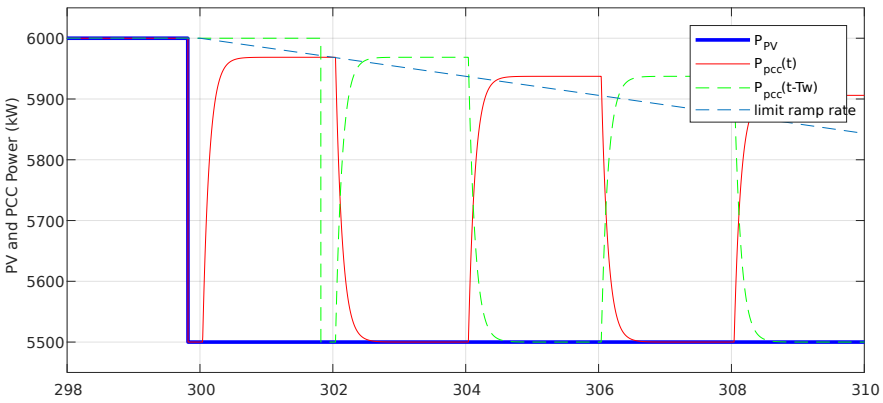


(b) Zoom on the above graph.

Figure 3.1: Results of simulation 1.

Every 2 seconds, the value of $P_{pv}(t)$ is compared to $P_{pcc}(t - T_w)$. At time $t = 300s$ (i.e. the first sam-

ple after the step), the current value of $P_{PV}$ is already 5500 kW, while the previous value of $P_{pcc}$ is 6000 kW. Therefore, to soften this sudden step-down event and restrict the power to the ramp rate limitation, the battery will inject power, therefore increasing $P_{pcc}$. The battery injects power within a characteristic time $\tau_{bat} = 100ms$.

Then, the green curve (value of $P_{pcc}$ 2 seconds before) remains at the value 6000 kW for a duration $T_w = 2s$. At $t = 302$s the same phenomenon than 2 seconds before occur, and the battery stops injecting power: $P_{pcc}(t)$ goes down again for the duration of one sample, before going up again for a duration $T_w$.

Therefore, oscillations can be observed in $P_{pcc}(t)$. The amplitude of these oscillations linearly decrease over time, controlled by the ramp rate limitation imposed on $P_{pcc}(t)$. Such oscillations can be described as a succession of "down" and "up" events. The duration of a "down" event is equal to the sampling time $T_s$, and the duration of a "up" event is $T_w$. Therefore, the oscillation period is here equal to $T_w + T_s = 4s$.

The other noticeable phenomenon in the results of this simulation is that the ramp-down event is finally 2 times slower than expected, with a duration of approximately 64s, while the expected duration given by equation 3.1 is approximately 32 seconds. This is confirmed by the fact that the "limit line" on the graph does not match the ramp-down curve.

This delay is due to the fact that the power is supposed to decrease of 15.67 kW per second, but it actually does it only during the "up" events, which represent a fraction $\frac{T_w}{T_s+T_w} = 50\%$ of the time. Therefore the ramp rate has to be corrected to take account of this delay:

$$RR'_{max} = \frac{T_s + T_w}{T_w} RR_{max} = 2RR_{max} = 20\%/\text{min} \tag{3.2}$$

**Simulation 2**

Simulation 2: $n = 4$, $T_w = 2$ s, $T_s = 500$ ms. The results are presented in Figure 3.2 (same quantities and colors than in Figure 3.1).

The same oscillation phenomenon than in the previous simulation can be observed. This second simulation confirms that the duration of the "down" events is one sample $T_s$ (except for the first one), while the "up" events last for a time window $T_w$, therefore the oscillation period is given by $T_s + T_w$ (2.5 seconds in this simulation).

Once again, the ramp-down event is longer than expected, and the ratio between the expected duration (about 31.9 seconds) and the actual duration is once again equal to $\frac{T_s+T_w}{T_w} = 2.5/2 = 1.25$. Therefore the ramp rate has to be corrected to take account of this delay:

$$RR'_{max} = \frac{T_s + T_w}{T_w} RR_{max} = 1.25RR_{max} = 12.5\%/\text{min} \tag{3.3}$$

**Simulation 3**

Simulation 3: $n = 10$, $T_w = 2$ s, $T_s = 200$ ms. The results are presented in Figure 3.3 (same quantities and colors than in Figure 3.1). The oscillation phenomenon has the same behaviour than in the two previous simulations: "down" events with a duration $T_s = 200$ ms and "up" events with duration $T_w = 2$ s. Once again, the ramp-down event is longer than expected, and the ratio between the expected duration (about 31.9 seconds) and the actual duration is once again equal to $\frac{T_s+T_w}{T_w} = 2.2/2 = 1.1$. Therefore the ramp rate has to be corrected to take account of this delay:

$$RR'_{max} = \frac{T_s + T_w}{T_w} RR_{max} = 1.1 RR_{max} = 11\%/\text{min} \tag{3.4}$$

### 3.1.3 Correcting the ramp rate limitation

As it was noticed before, a simple way of dealing with the delays caused by this oscillation phenomenon is to multiply the maximum and the minimum ramp rate by the $\frac{T_s+T_w}{T_w}$, because the oscillation period is given by $T_s + T_w$ instead of the expected value $T_w$. The results of the corrected versions of simulations 1, 2 and 3 are presented in Figure 3.4. These corrected versions of these simulations comply with the minimum ramp rate and have the correct duration (about 31 seconds, see equation 3.1).

### 3.1.4 Influence of battery dynamics $\tau_{bat}$

Simulation 3 (the corrected version that comply with the limit ramp rate) is carried out another time, but with faster battery dynamics: $\tau_{bat} = 50ms$ instead of $\tau_{bat} = 100ms$. Results are presented in Figure 3.5.

By comparing Figure 3.5 and Figure 3.4c, it can be observed that the only change implied by the different value of $\tau_{bat}$ is that $P_{bat}(t)$ and $P_{pcc}(t)$ reach their maximal value faster during the "up" events (but the total duration of these events is still the same, $T_s$). Consequently, having a battery with slower or faster dynamics will not influence this oscillation phenomenon.

### 3.1.5 Filtering oscillations

Is has been shown that whatever is the value of the ratio $T_w/T_s$, and taking into account the battery dynamics $\tau_{bat}$, $P_{pcc}(t)$ and $P_{bat}(t)$ will oscillate. In order to avoid these oscillations, a solution is to apply a low-pass filter on $P_{PCC}(t)$. The time constant $T_d$ of this filter should be greater than $T_s + T_w$, so that the oscillations can be correctly filtered. Setting $T_d = T_s + T_w$, simulation 3 is carried out again with a first-order filter of time constant $T_d$ on $P_{pcc-meas}(t)$.

The principle of the ramp rate limitation, with mention of the filter, is shown in Figure 3.6.

The results are presented in figure 3.7a. Only the first "down" event and the beginning of the second one remain, while all the next oscillations have been correctly removed. $P_{pcc}(t)$ now decreases following a ramp rate. But once again, it seems that the power variation is not limited by the expected ramp rate. This is due to the fact that the filtering delays the signal and therefore slows down the power decrease. Therefore the ramp rate should be corrected a second time, by replacing $T_w + T_s$ by $T_w + T_s + T_d = 2(T_w + T_s)$ in equation 3.4. The results of the simulation after applying this corrected limit ramp rate are shown in figure 3.7b.

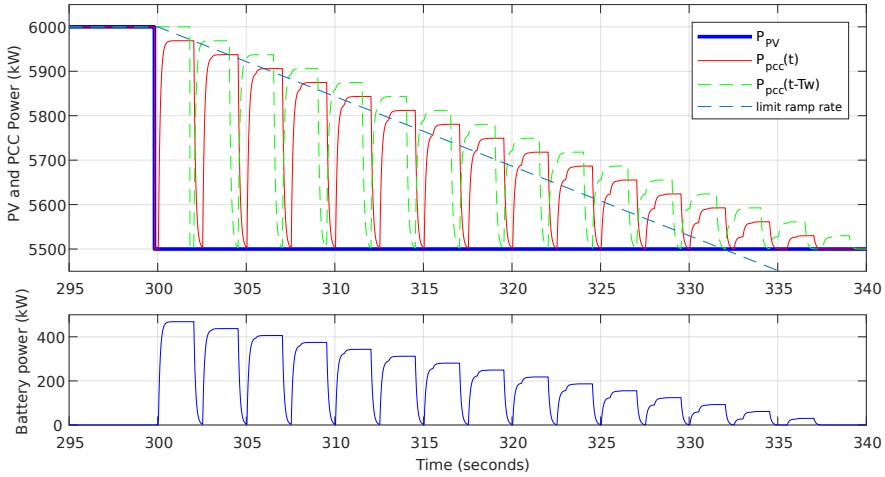


(a) Results of simulation 2: PV power and power delivered at the PCC (top) and power delivered by the battery (bottom).

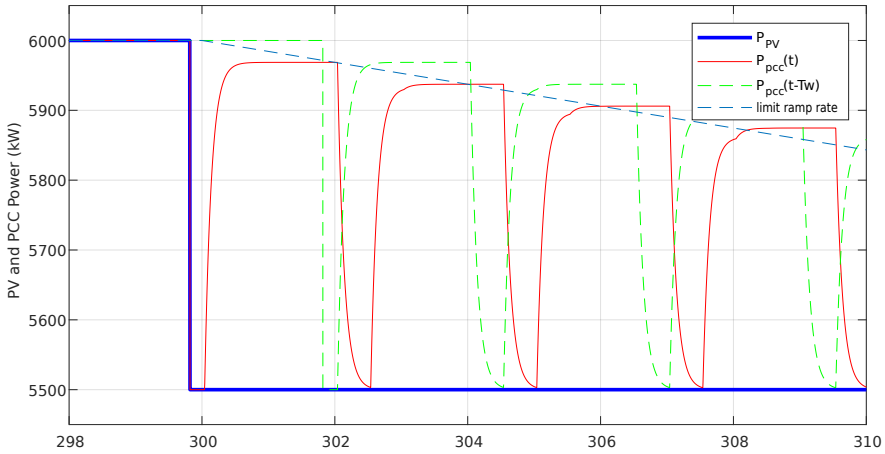


(b) Zoom on the above graph.

Figure 3.2: Results of simulation 2.

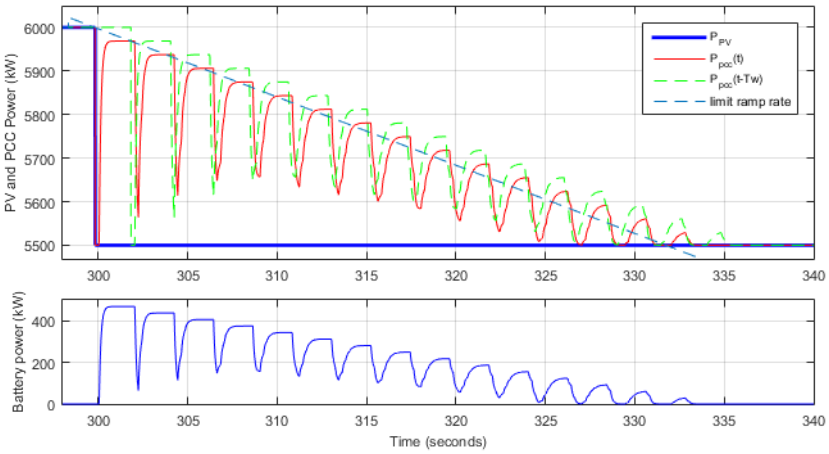


(a) Results of simulation 3: PV power and power delivered at the PCC (top) and power delivered by the battery (bottom).

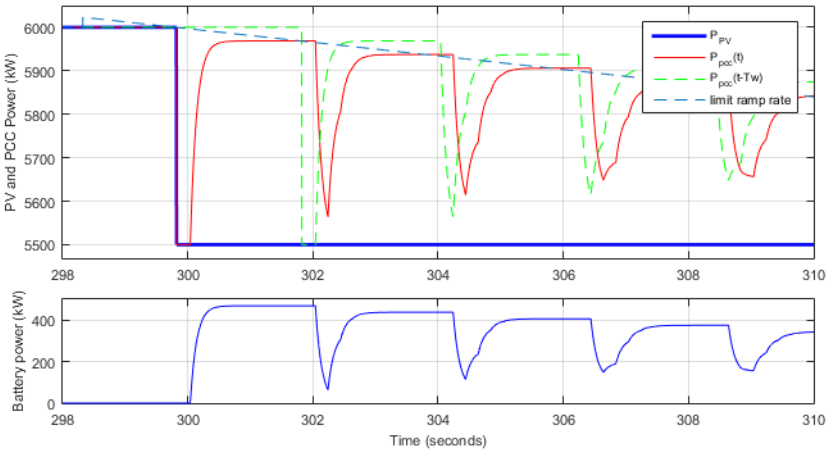


(b) Zoom on the above graph.

Figure 3.3: Results of simulation 3.

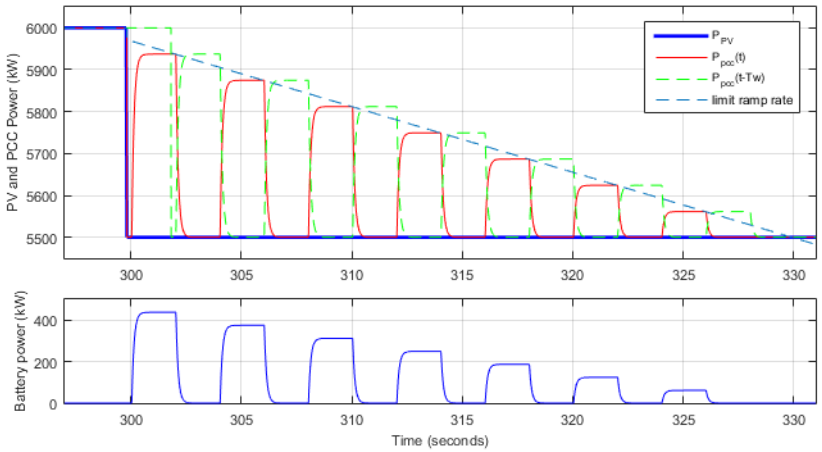


(a) Results of corrected simulation 1.

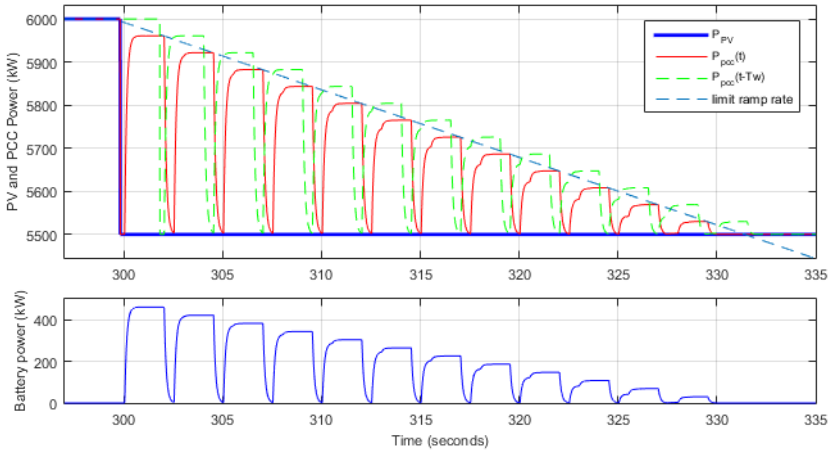


(b) Results of corrected simulation 2.

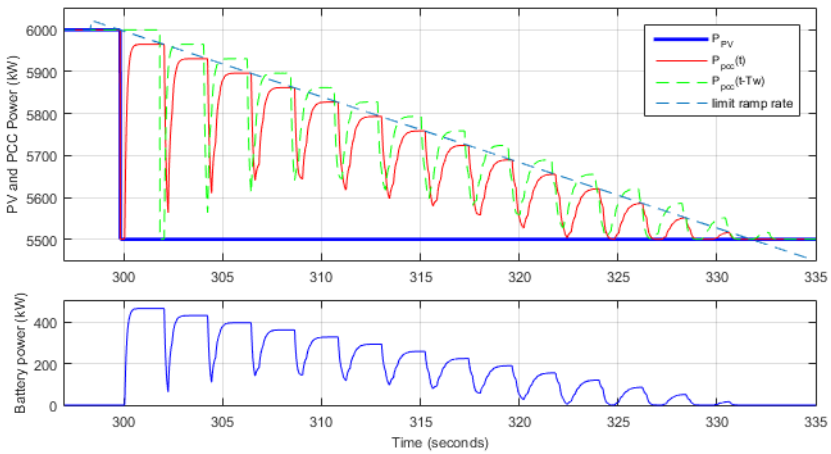


(c) Results of corrected simulation 3.

Figure 3.4: Results of corrected simulations 1, 2 and 3.

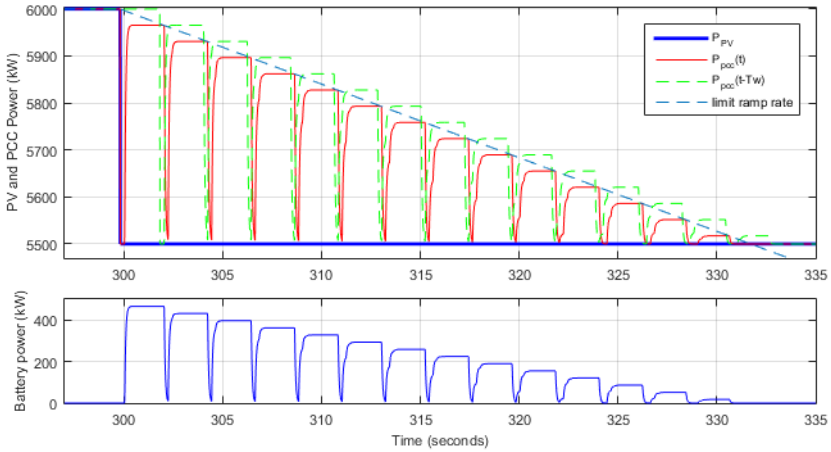


Figure 3.5: Results of simulation 3 with different battery dynamics ($\tau_{bat} = 50$ ms instead of $\tau_{bat} = 100$ ms).

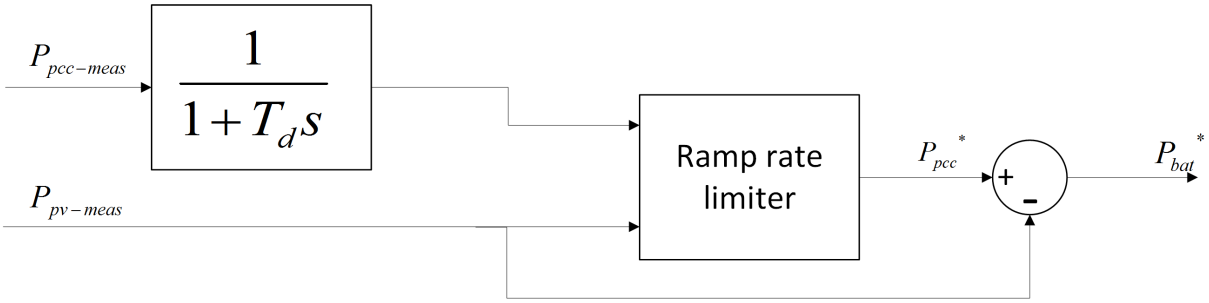


Figure 3.6: Principle of the ramp rate control, with a filter on $P_{pcc-meas}(t)$.

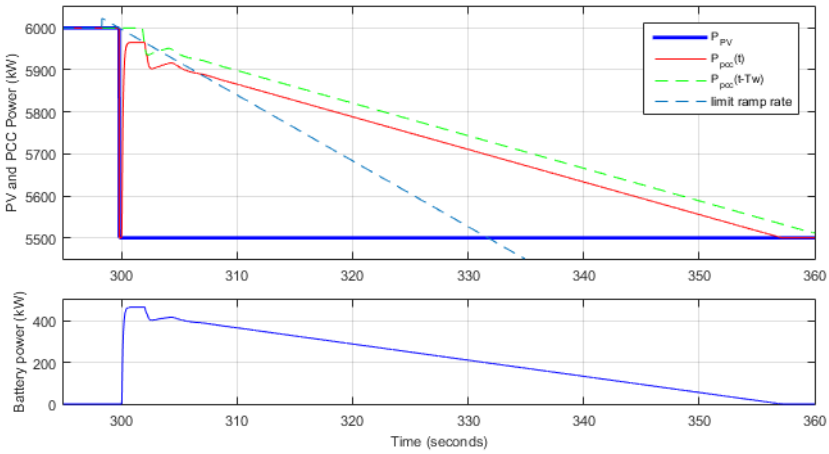


(a) Results of simulation 3 with a filter that has a time constant $T_d = T_w + T_s = 2.2$ s.

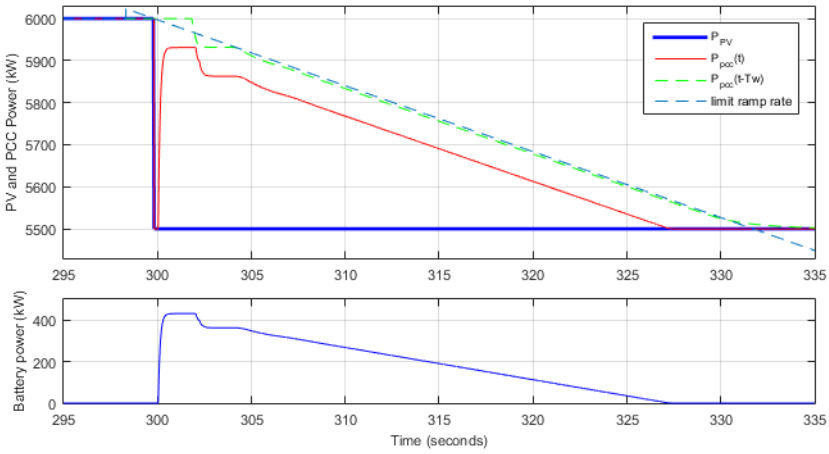


(b) Results of simulation 3 with a filter that has a time constant $T_d = T_w + T_s = 2.2$ s, and correcting the ramp rate again.

Figure 3.7: Results of simulation 3 with a filter on $P_{pcc-meas}(t)$.

## 3.2 SOC control implementation; response to a real PV profile

Figure 3.8 shows the results obtained during a Simulink simulation over 30 minutes, with the following elements:

- Ramp rate control on $P_{pcc}(t)$ (see section 2.2);
- Filter on $P_{pcc-meas}(t)$ to avoid undesirable power oscillations (see section 3.1.5);
- Proportional controller on $SOC(t)$ with a gain $K_{SOC} = 1000$ (see equation 2.7).

By observing the SOC curve (bottom graph in Figure 3.8), one can see that the SOC is almost always between the chosen bounds (0.4 and 0.6), which means that the value $K_{SOC} = 1000$ for the gain of the proportional controller is adapted to the model.

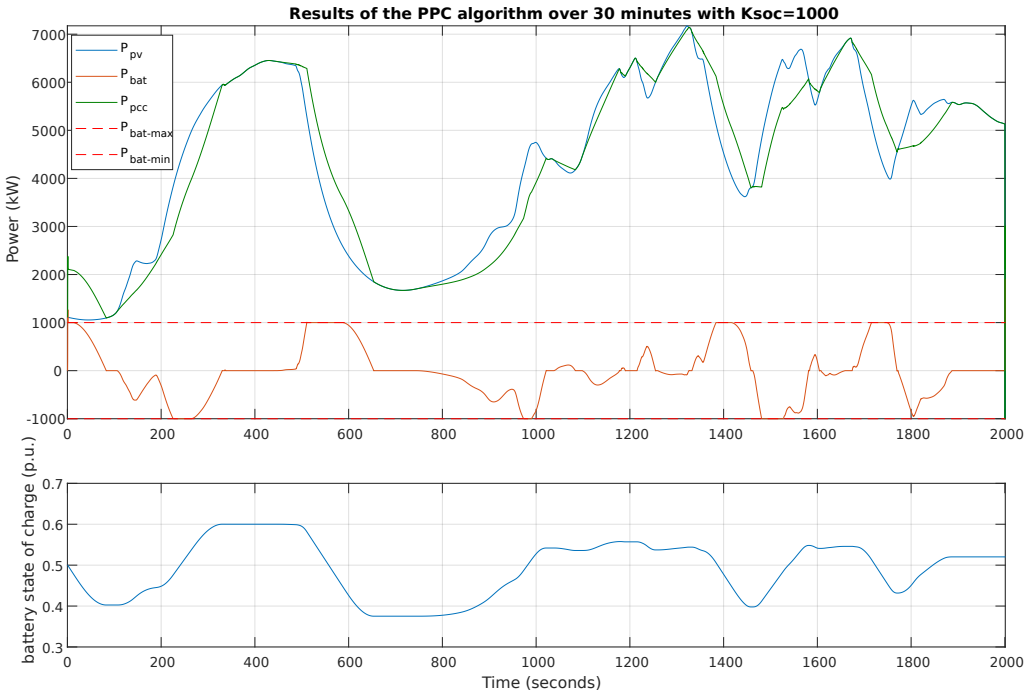


Figure 3.8: Results of the PPC algorithm simulation over 30 minutes.

Figure 3.9 shows the evolution of the final ramp rate with time, and also the statistical distribution of this quantity. One can see that, although the ramp rate control is quite efficient, on the contrary to Figure 2.8 that showed the result in the ideal case, the final ramp rate is not always between the fixed bounds $\pm 10\%/\text{min}$ of the nameplate plant power. This difference between the ideal case and the real case is essentially due to the following factors:

- The battery and the PV dynamics make them not apply immediately the setpoints they receive;

- There are measurements and sending delays;
- The battery has a maximum absorbing/delivering power. One can see on the top graph in Figure 3.8 that the battery power (orange curve) reached its maximum and its minimum value ($\pm$1000 MW) several times during the experiment.
- The SOC proportional controller affects the ramp rate limitation (see equations 2.8).

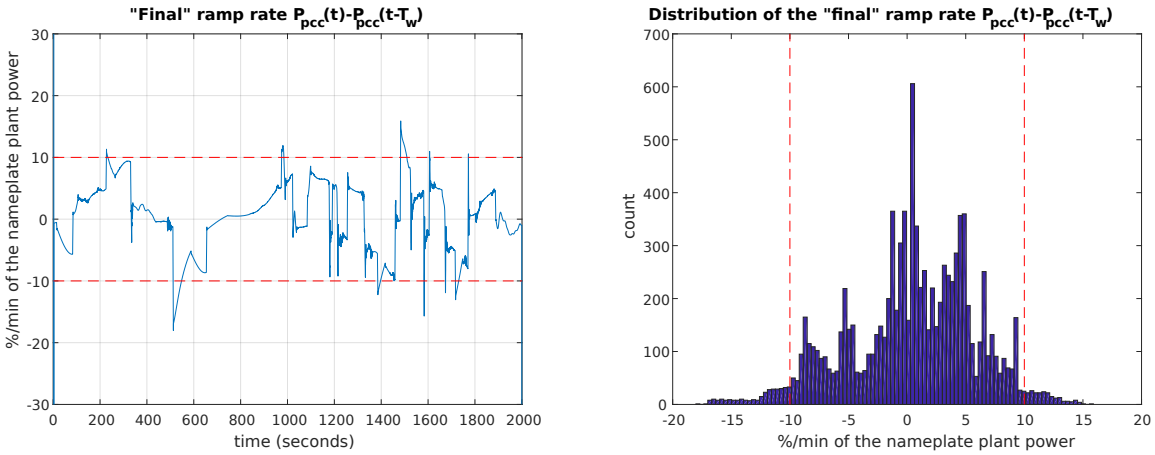


(a) Evolution of the ramp rate with time.

(b) Ramp rate statistical distribution.

Figure 3.9: Final ramp rate after application of the PPC algorithm: evolution with time and statistical distribution.

## 3.3 Conclusion

Carrying out simulations in Simulink was helpful to validate the plant model and the PPC algorithm. Moreover, it allowed to anticipate an intrinsic issue of the algorithm (the power oscillations observed in section 3.1) and to propose a solution for this problem (the filter considered in paragraph 3.1.5). It also allowed to test the SOC proportional controller, and to provide an insight of what would be the result of the PPC algorithm on a real, non-ideal hybrid PV-battery power plant. Even though the ramp rate and the battery SOC are not *always* between the fixed bounds ($\pm 10\%/\text{min}$ of the nameplate plant power for the ramp rate, $0.4 - 0.6$ for the SOC), they most often comply to these limits, which means that the PPC algorithm is efficient.

# Chapter 4

# Implementing the PPC on a scaled emulation platform

The PPC algorithm developed in this work was tested on a scaled platform that emulates the behavior of a real hybrid PV-battery power plant.

## 4.1 The approach of emulation in the energy research sector

Emulation consists in using devices called emulators, that imitate the behavior and the dynamics of real power devices, such as:

- power sources: PV panels, wind turbines, etc.
- storage devices: batteries, flywheels, fuel cells, electric vehicles, etc.
- DC or AC loads.

Note that any emulator require the use of a power source. Indeed, an emulator that would emulate a PV panel needs to actually produce power as if it was a PV panel, and therefore requires a power source to produce this power: for instance a diesel generator, or the external grid can serve as a power supply. Conversely, an emulator emulating a load needs to be able to actually consume power as if it was a real load. A battery emulator should be able to both produce and consume power, as would do a real battery.

An emulator has two layers, a software layer and a hardware layer. The conditions of the experiment are imposed by the user (for instance, weather conditions or load consumption profile), and the software layer computes the system variables that the real system would show under the same conditions, whereas the hardware layer imposes to the system the calculated variables by means of mechanical, electric or electronic devices.
For instance, in the case of a PV panel emulator, the user can input an irradiance profile and the software layer will calculate the active power generation based on the real DC voltage measurement. Then, the role of the hardware layer is to actually produce this active power at the terminals of the PV panel emulator, using the power source of the emulator (diesel generator for instance).

The paper [16] carries out a comprehensive review of the existing emulators in the energy sector, and provides a detailed state of the art of the emulation in the literature.

## 4.2 Presentation of the emulation platform

The CITCEA-UPC emulation platform consists of the following elements:

- a PV panel emulator;
- a battery emulator;
- an inverter for the PV panel emulator;
- an inverter for the battery emulator;
- a load emulator (that was not used in this work);
- a diesel emulator;
- a communication system using Ethernet cables;
- a computer to control the platform, collect the measurements and send the appropriate setpoints. It can be called more formally a SCADA device (SCADA = "Supervisory control and data acquisition").

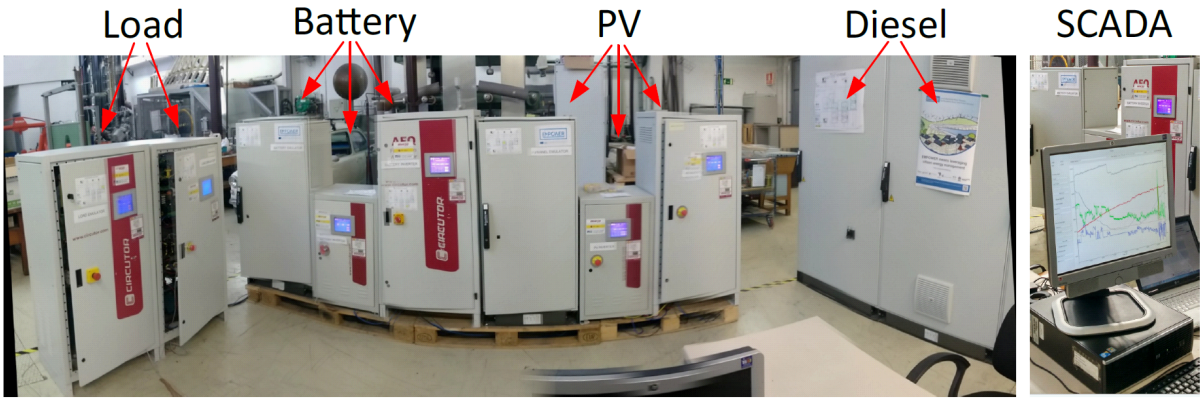


Figure 4.1: Microgrid photo. SCADA = "Supervisory control and data acquisition".

The microgrid general scheme is shown in Figure 4.2. The platform can be either connected or disconnected to the grid. The nameplate power of the PV panel emulator is 1800 W, therefore the PV power profiles passed to this emulator had to be scaled down to be consistent with this value. To carry out this scale-down, the arbitrary choice that was made was to decide that the maximum value of the PV profile passed to the PV panel emulator was exactly 1800 W.

During this work, only the PV panel emulator, the battery emulator and their two associated inverters were used (and obviously the diesel generator to provide power). The rest of the platform was not used.

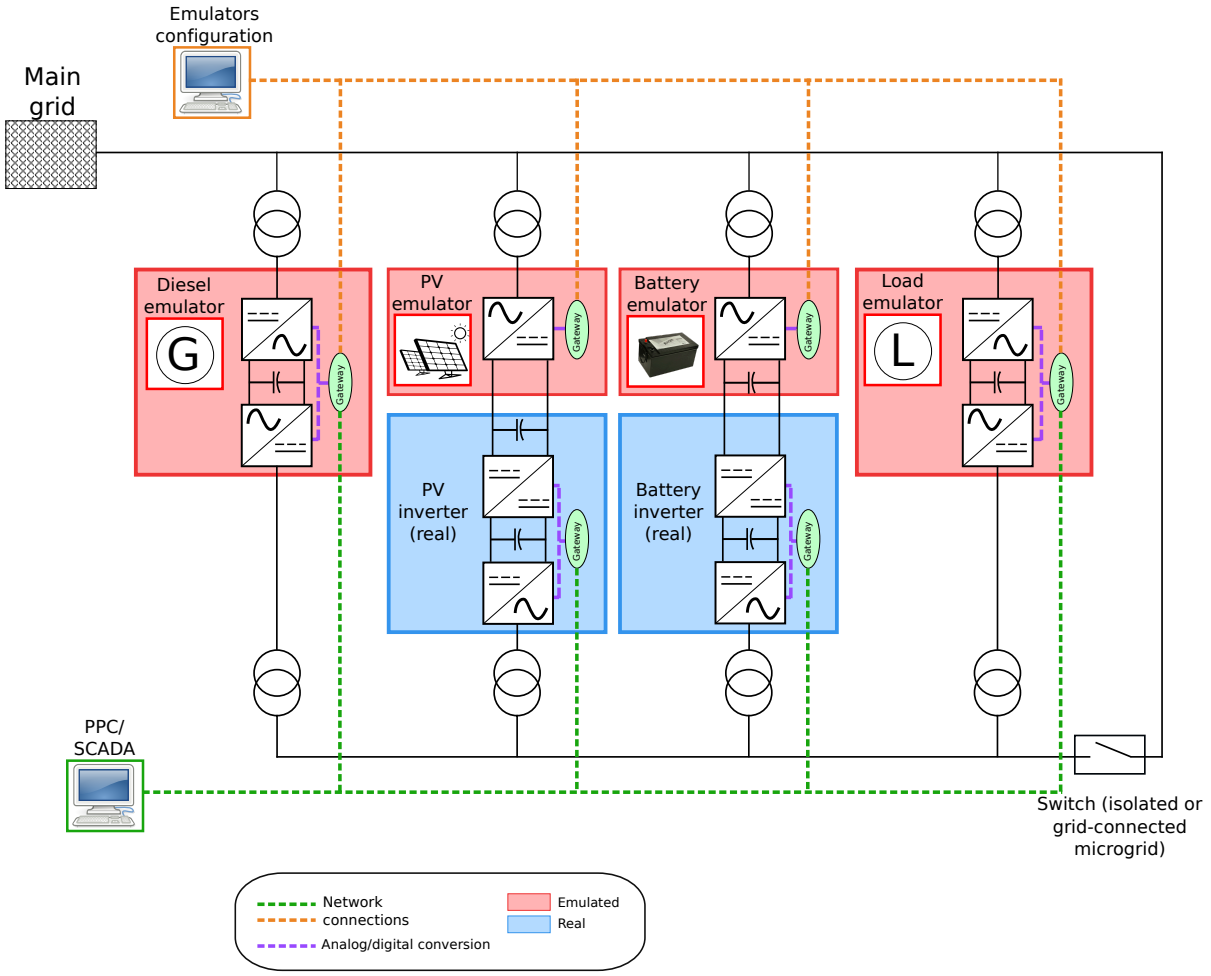


Figure 4.2: Microgrid emulator scheme. SCADA = "Supervisory control and data acquisition", PPC = "Power Plant Controller".

## 4.3 Implementation of the PPC algorithm on the emulation platform

To interact with the emulation platform, a MATLAB real-time routine was used. A real-time routine consists in receiving data and sending data through the modbus network of the microgrid at regular intervals of time, namely $T_s = 0.2$ s in this case. The principle of the use of the platform to implement the Ramp Rate Control through a MATLAB real-time routine is presented in the flowchart of Figure 4.3. All of the operations presented in this flowchart are carried out every $T_s = 0.2$ s.

## 4.4 Ramp rate control testing

The same PV profile that the one used during the simulations was used. However it was scaled down to match the nameplate power of the PV emulator, that is 1800 W. The results of the emulation are

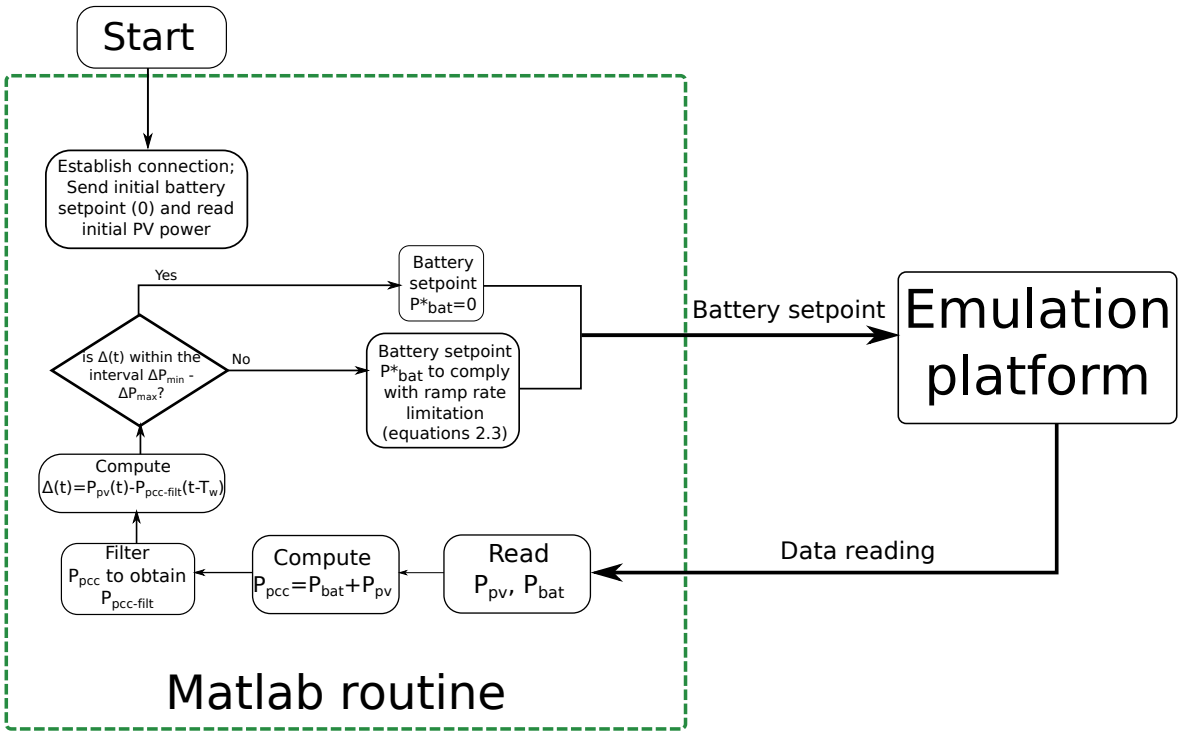


Figure 4.3: Flowchart describing the MATLAB real-time routine interacting with the emulation platform for applying the ramp rate limitation.

presented in Figure 4.4.

By observing the curves, it is clear that the ramp-up events are correctly treated. In particular the two first ramp-up events happening between times 200 and 500 seconds are perfectly treated by the PPC algorithm. However, the ramp-down events are not treated very correctly by the algorithm. For instance, one can see that during the ramp-down event starting at time 500 seconds, the power sent to the grid (green curve) starts decreasing at the limit ramp rate, but then the decreasing slows down around time 700 seconds. This is probably due to the filter.

After time 1000 seconds, several small down-events in the photovoltaic power (blue curve) occur, and one can notice during these events the battery provides power so that the final power $P_{pcc}(t)$ remains almost constant. This was unexpected but it is a good thing for the grid because it means that the provided power is very stable, almost "flat", during these short down-events. It probably happened because of a too intense filtering of $P_{pcc}(t)$.

As for what happens after time 1800, however, it has no rational reason to happen. One can see that the PV power is more or less stable after this event but the battery power keeps on increasing, and as a result the PCC power remains significantly higher than the PV power.

Figure 4.5 shows, as usual, both for the "natural" ramp rate and the "final" ramp rate after application

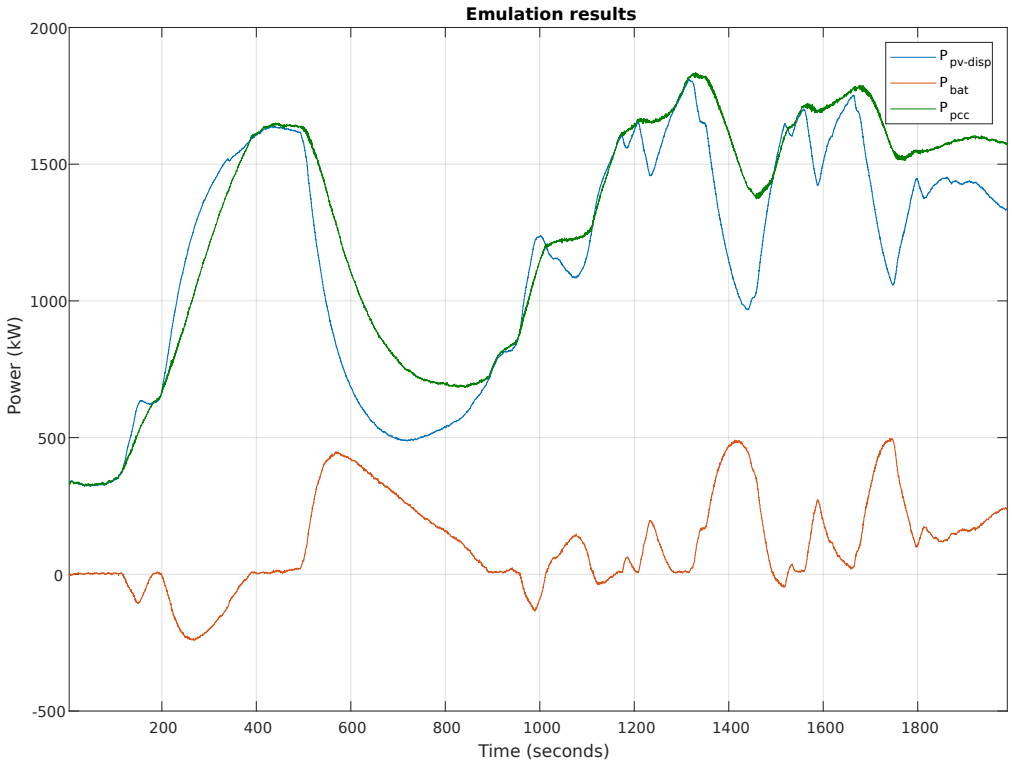


Figure 4.4: Results of the PPC algorithm emulation over 30 minutes.

of the PPC algorithm, the evolution with time and the statistical distribution. The final ramp rate distribution is indeed less extended that the initial ramp rate distribution, but the results are less conclusive than with the simulations in Simulink. This is due to several factors:

- The platform is not calibrated perfectly, there are some losses in the converters. For instance, when a setpoint $P^*_{bat} = 0$ W is sent to the battery, most of the time the battery will not produce 0 W but 10 or 15 W. Moreover, the power that will be produced by the battery for a given setpoint is not always the same, which makes calibration difficult.

- Since the nameplate power of the PV panel emulator is $P_{nom} = 1800$ W, the maximum ramp rate is 180 W/min i.e. 6 W every 2 seconds. This is problematic because 6 W is a value which has the same order of magnitude that the "noise", i.e. the fluctuations that can be observed in the power produced by the battery and the PV emulator. This means that the noise itself can trigger the ramp rate limitation, which has obvious consequences on the control efficiency.

- The discrete low-pass filter was difficult to implement because it tends to slow-down the variations if the filter time constant is too high. This phenomenon is illustrated in Figure 4.6. A step signal with noise was filtered for several time constant values, and then was applied the ramp rate limitation. For the higher values of the time constant (for instance $T_d = 500$ s, light green curve), one can observe that although the noise is more efficiently filtered, the step is transformed into

a decreasing exponential function. As a result, after a certain time, the slope of the exponential becomes smaller than the limit slope, which means that the signal no longer follows the maximal allowed slope. As a result the decreasing of the signal is delayed. This is probably what happened during the emulations, which explains that the signal was always very late to the septpoint and did not have the time to "follow" the short events. But less filtering would have meant not being able to get rid of the noise.

An emulation was carried out with a PV step power profile, and the results (presented in Figure 4.7), confirm that this phenomenon is at stake. Indeed, one can see that the first observations are soon filtered (it was the same during the Simulink simulations), but on the contrary of what happened during the simulations, the slope of the curves tends not remain constant but to go down, following a decreasing exponential instead of following a straight line.

## 4.5 SOC control testing

Due to the battery emulator configuration, there is a minimum battery capacity. This minimum capacity is too large in comparison to the required power. As a result, the current platform is not adequate for testing the SOC control.

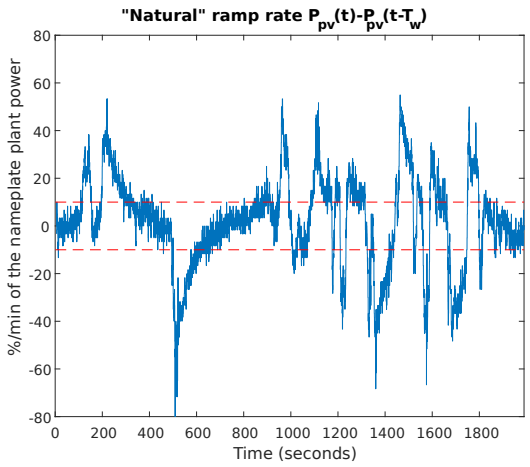


(a) "Natural" ramp rate calculated from the PV profile.

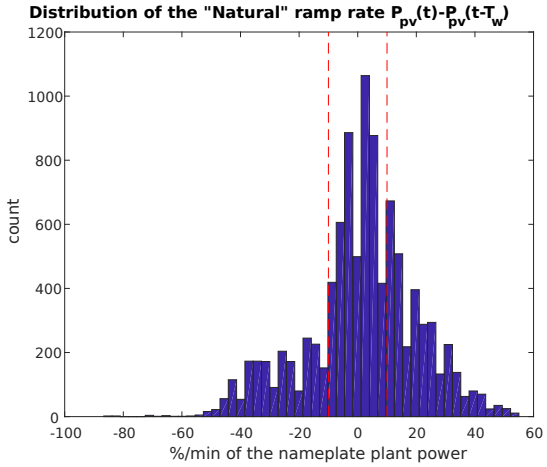


(b) Distribution of the "natural" ramp rate.

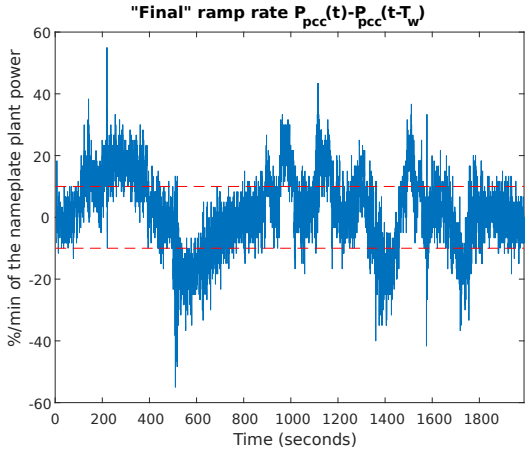


(c) "Final" ramp rate after application of the ramp rate limitation.

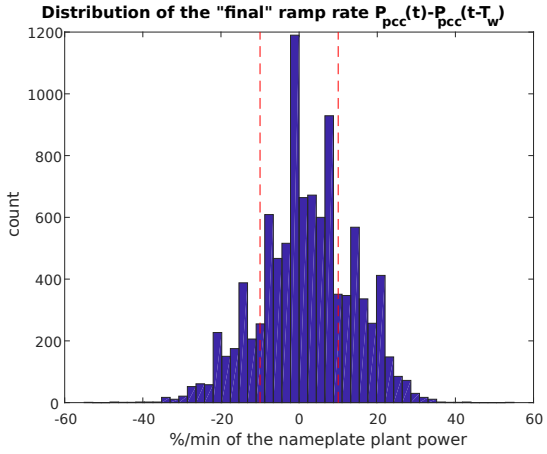


(d) Distribution of the "final" ramp rate.

Figure 4.5: Comparison of the ramp rates (evolution with time, and statistical distribution) without the ramp rate limitation (4.5a, 4.5b) and with the ramp rate limitation (4.5c, 4.5d).

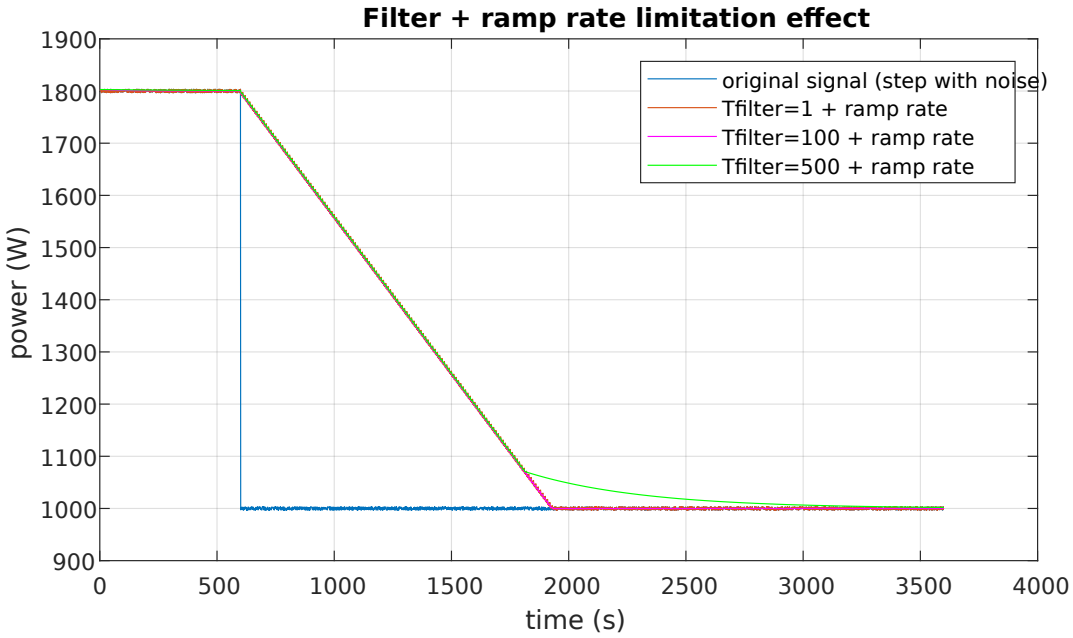


Figure 4.6: Filtering and ramp rate limitation of a step signal with noise, for different values of the filter time constant.

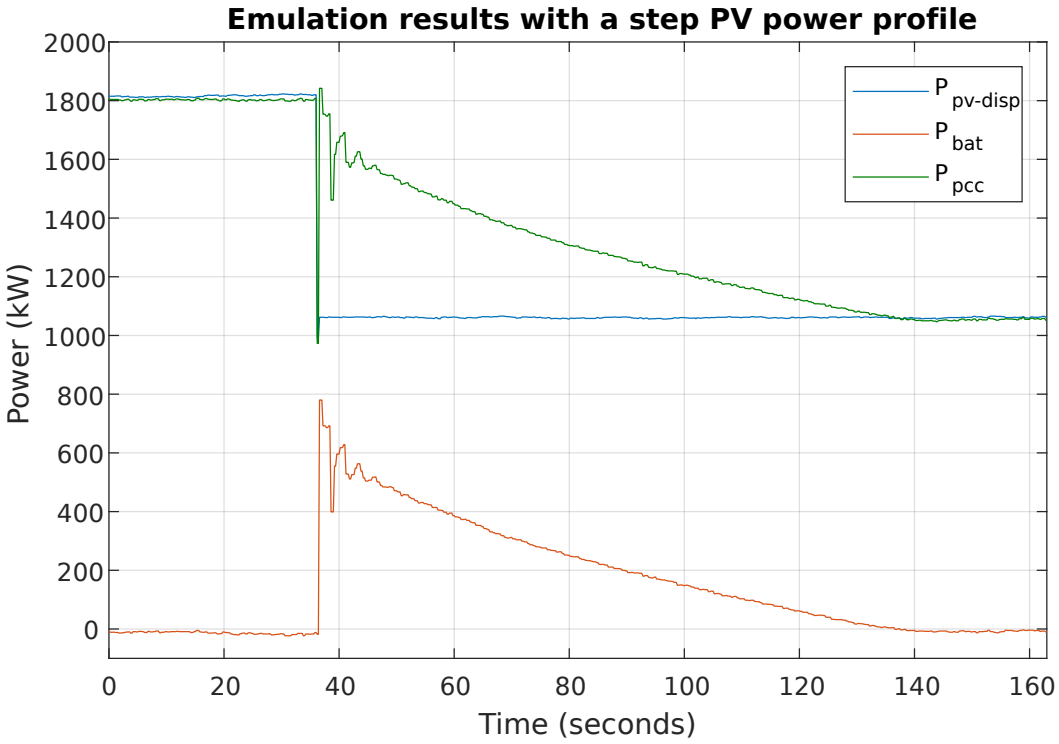


Figure 4.7: Emulation results with a step PV power profile.

# Chapter 5

# Conclusion

By the means of simulations in Simulink, the PPC algorithm presented in this work is proven to be efficient and to provide a proper ramp rate limitation, and to properly control the battery state of charge in order not to carry out too deep battery cycles. The ramp rate limitation is also tested on the scaled microgrid emulation platform, and is proven to limit the instantaneous ramp rate, but not enough to comply with the grid codes requirements. The potential reasons for these ambivalent results were explained in section 4.4. The power oscillations produced by the ramp rate controller have been identified and characterized. Thanks to this analysis, a solution based on filtering has been proposed showing its efectiveness.

**Future works:**

- Solve the filtering issues that slow down the ramp rate;
- Find a solution so that the maximum/minimum power over a time window $T_w$ is not as small as the "noise" of the emulator.
- Once the two previous points are solved, add the SOC control to the code interacting with the platform.
- Add other functionalities such as power curtailment, reactive power control, voltage/frequency regulation, etc.

# Bibliography


[1] Eurostat. *Supply, transformation and consumption of electricity - annual data*. URL: http://appsso.eurostat.ec.europa.eu/nui/show.do?dataset=nrg_105a&lang=en.

[2] Eurostat. *Share of renewable energy in gross final energy consumption*. URL: http://ec.europa.eu/eurostat/tgm/graph.do?tab=graph&plugin=1&pcode=t2020_31&language=en&toolbox=type.

[3] Wikimedia commons. *From a solar cell to a PV system - illustration*. URL: https://commons.wikimedia.org/wiki/File:From_a_solar_cell_to_a_PV_system.svg.

[4] International Energy Agency. *Trends 2016 in photovoltaic applications*. Tech. rep. 21. International Energy Agency, 2016. URL: http://www.iea-pvps.org/fileadmin/dam/public/report/national/Trends_2016_-_mr.pdf.

[5] Ignacio J. Perez Arriaga, Hugh Rudnick, and Michel Rivier. *Electric Energy Systems. Analysis and Operation*. CRC Press, July 11, 2008. 648 pp. ISBN: 9780849373657. URL: http://www.ebook.de/de/product/7697287/electric_energy_systems_analysis_and_operation.html.

[6] Ana Cabrera-Tobar et al. "Review of advanced grid requirements for the integration of large scale photovoltaic power plants in the transmission system". In: *Renewable and Sustainable Energy Reviews* 62 (2016), pp. 971–987. DOI: 10.1016/j.rser.2016.05.044.

[7] National Energy Regulator of South Africa (NERSA). *Grid connection code for Renewable power plants connected to the electricity transmission system or the distribution system in South Africa*. Tech. rep. National Energy Regulator of South Africa (NERSA), 2014. URL: http://www.nersa.org.za/Admin/Document/Editor/file/Electricity/TechnicalStandards/South%20African%20Grid%20Code%20Requirements%20for%20Renewable%20Power%20Plants%20-%20Version%202%208.pdf.

[8] Romanian Power Grid Company Transelectrica SA. *Technical transmission grid code of the Romanian Power System*. Tech. rep. Romanian Power Grid Company Transelectrica SA, 2004. URL: http://www.transelectrica.ro/documents/10179/33158/cod_ret_en.pdf/3b005f38-ab88-440a-b446-cbe8e79bcbe1.

[9] Puerto Rico Electric Power Authority. *Minimum technical requirements for interconnection of photovoltaic facilities*. Tech. rep. Puerto Rico Electric Power Authority, 2012. URL: http://solar.ucsd.edu/nguyen/PREPArequirements.pdf.

[10] Ben Noone. *PV Integration on Australian distribution networks - literature review*. Tech. rep. The Australian PV Association, Sept. 2013. URL: http://ceem.unsw.edu.au/sites/default/files/documents/APVA%20%20PV%20and%20DNSP%20Literature%20review%20September%202013.pdf.

[11] E. Bullich-Massagué et al. "Power plant control in large-scale photovoltaic plants: design, implementation and validation in a 9.4 MW photovoltaic plant". In: *IET Renewable Power Generation* 10.1 (2016), pp. 50–62. DOI: 10.1049/iet-rpg.2015.0113. URL: https://doi.org/10.1049%2Fiet-rpg.2015.0113.

[12] E. Bullich-Massagué et al. "Active power control in a hybrid PV-storage power plant for frequency support". In: *Solar Energy* 144 (2017), pp. 49–62. DOI: 10.1016/j.solener.2016.12.033. URL: https://doi.org/10.1016%2Fj.solener.2016.12.033.

[13] MJE Alam, KM Muttaqi, and D Sutanto. "A novel approach for ramp-rate control of solar PV using energy storage to mitigate output fluctuations caused by cloud passing". In: *IEEE Transactions on Energy Conversion* 29.2 (2014), pp. 507–518.

[14] Rob van Haaren, Mahesh Morjaria, and Vasilis Fthenakis. "An energy storage algorithm for ramp rate control of utility scale PV (photovoltaics) plants". In: *Energy* 91 (2015), pp. 894–902. DOI: 10.1016/j.energy.2015.08.081. URL: https://doi.org/10.1016%2Fj.energy.2015.08.081.

[15] Mathworks. *Simulink presentation*. URL: https://www.mathworks.com/products/simulink.html.

[16] E. Prieto-Araujo et al. "Renewable energy emulation concepts for microgrids". In: *Renewable and Sustainable Energy Reviews* 50 (2015), pp. 325–345. DOI: 10.1016/j.rser.2015.04.101.

# Appendix A: Budget

| Material | Unit cost (€) | Number of units | Total cost (€) |
|---|---|---|---|
| ASUS N751-JK laptop | 1700 | 0.1 | 170 |
| Desktop PC (at home) + screen | 700 | 0.1 | 70 |
| MATLAB+Simulink student license | 70 | 1 | 70 |
| **Materials subtotal** | | | **310** |

**Labour:** 16 weeks x 5 days/week x 5 hours/day = 400 hours, charged 30€each, which leads to a labour subtotal of **12 000**€.

| Designation | Rate | Total cost (€) |
|---|---|---|
| Materials subtotal | | 310 |
| Labour subtotal | | 12 000 |
| **Subtotal** | | **12 310** |
| Operational costs | 10% of the subtotal | 1 231 |
| Total without taxes | | 13 541 |
| Taxes | 21% | 2 843.61 |
| **Total, taxes included** | | **16 384.61** |

This budget is valid for a period of 3 months following its publication.

**Publication date:** June 21st, 2017
**Signature:** Robin Bourgeon

# Appendix B: Environmental impact

This project had no direct environmental impact, except the electricity consumption of the computers and of the emulation platform. However, a power plant control algorithm is useful to facilitate the integration of photovoltaic plants to the grid. As a result, the application of this algorithm at a utility scale should increase the renewables share in the energy mix, and therefore reduce the use of conventional power sources, including CO2-emitting sources such as coal and gas power plants, and also nuclear power.